3-1-2022

The Origin and Contribution of Cancer-Associated Fibroblasts in Colorectal Carcinogenesis

Hiroki Kobayashi
Adelaide Medical School

Krystyna A. Gieniec
Adelaide Medical School

Tamsin R.M. Lannagan
Adelaide Medical School

Tongtong Wang
Adelaide Medical School

Naoya Asai
Fujita Health University Graduate School of Medicine

See next page for additional authors

Gastroenterology 2022;162:890–906

The Origin and Contribution of Cancer-Associated Fibroblasts in Colorectal Carcinogenesis

Hiroki Kobayashi,[1,2,3,4,*] **Krystyna A. Gieniec**,[1,2,*] **Tamsin R. M. Lannagan**,[1,2,*] Tongtong Wang,[1,2] Naoya Asai,[5] Yasuyuki Mizutani,[3,6] Tadashi Iida,[3,6] Ryota Ando,[3] Elaine M. Thomas,[1,2] Akihiro Sakai,[3] Nobumi Suzuki,[1,2,7] Mari Ichinose,[1,2] Josephine A. Wright,[2] Laura Vrbanac,[1,2] Jia Q. Ng,[1,2] Jarrad Goyne,[1,2] Georgette Radford,[1,2] Matthew J. Lawrence,[8] Tarik Sammour,[1,2,8] Yoku Hayakawa,[7] Sonja Klebe,[9] Alice E. Shin,[10] Samuel Asfaha,[11] Mark L. Bettington,[12,13,14] Florian Rieder,[15,16] Nicholas Arpaia,[17,18] Tal Danino,[18,19] Lisa M. Butler,[1,2] Alastair D. Burt,[1,20] Simon J. Leedham,[21] Anil K. Rustgi,[18] Siddhartha Mukherjee,[22] Masahide Takahashi,[3,4,23] Timothy C. Wang,[22] Atsushi Enomoto,[3] Susan L. Woods,[1,2] and Daniel L. Worthley[2,24]

[1]Adelaide Medical School, University of Adelaide, Adelaide, South Australia, Australia; [2]South Australian Health and Medical Research Institute (SAHMRI), Adelaide, South Australia, Australia; [3]Department of Pathology, Nagoya University Graduate School of Medicine, Nagoya, Aichi, Japan; [4]Division of Molecular Pathology, Center for Neurological Disease and Cancer, Nagoya University Graduate School of Medicine, Nagoya, Aichi, Japan; [5]Department of Molecular Pathology, Graduate School of Medicine, Fujita Health University, Toyoake, Aichi, Japan; [6]Department of Gastroenterology and Hepatology, Nagoya University Graduate School of Medicine, Nagoya, Aichi, Japan; [7]Department of Gastroenterology, Graduate School of Medicine, University of Tokyo, Tokyo, Japan; [8]Colorectal Unit, Department of Surgery, Royal Adelaide Hospital, Adelaide, South Australia, Australia; [9]Department of Anatomical Pathology, Flinders Medical Centre, Bedford Park, Adelaide, South Australia, Australia; [10]Pathology and Laboratory Medicine, Schulich School of Medicine and Dentistry, University of Western Ontario, London, Ontario, Canada; [11]Department of Medicine, University of Western Ontario, London, Ontario, Canada; [12]Envoi Specialist Pathologists, Kelvin Grove, Queensland, Australia; [13]Faculty of Medicine, University of Queensland, Herston, Queensland, Australia; [14]QIMR Berghofer Medical Research Institute, Herston, Queensland, Australia; [15]Department of Gastroenterology, Hepatology, and Nutrition, Digestive Diseases and Surgery Institute, Cleveland Clinic Foundation, Cleveland, Ohio, USA; [16]Department of Inflammation and Immunity, Lerner Research Institute, Cleveland Clinic Foundation, Cleveland, Ohio, USA; [17]Department of Microbiology and Immunology, Vagelos College of Physicians and Surgeons, Columbia University, New York, New York, USA; [18]Herbert Irving Comprehensive Cancer Center, Columbia University, New York, New York, USA; [19]Department of Biomedical Engineering, Columbia University, New York, New York, USA; [20]Translational and Clinical Research Institute, Newcastle University, Newcastle upon Tyne, United Kingdom; [21]Intestinal Stem Cell Biology Lab, Wellcome Trust Centre Human Genetics, University of Oxford, Oxford, United Kingdom; [22]Department of Medicine and Irving Cancer Research Center, Columbia University, New York, New York, USA; [23]International Center for Cell and Gene Therapy, Fujita Health University, Toyoake, Aichi, Japan; and [24]GastroIntestinal Endoscopy, Lutwyche, Queensland, Australia

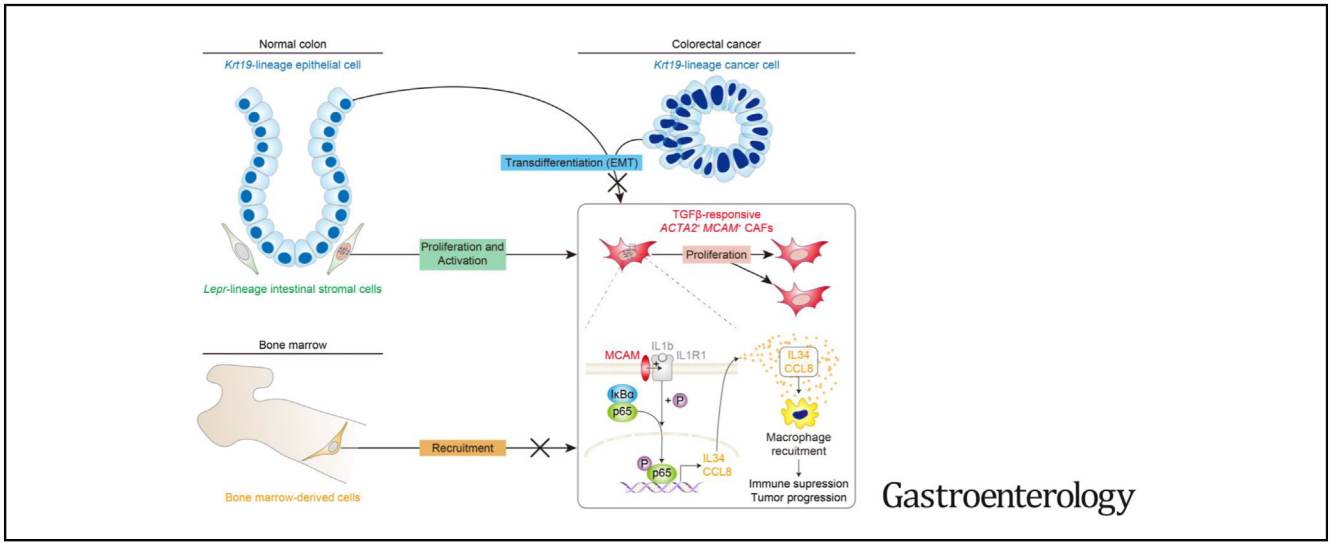

See Covering the Cover synopsis on page 666.

BACKGROUND & AIMS: Cancer-associated fibroblasts (CAFs) play an important role in colorectal cancer (CRC) progression and predict poor prognosis in CRC patients. However, the cellular origins of CAFs remain unknown, making it challenging to therapeutically target these cells. Here, we aimed to identify the origins and contribution of colorectal CAFs associated with poor prognosis. **METHODS:** To elucidate CAF origins, we used a colitis-associated CRC mouse model in 5 different fate-mapping mouse lines with 5-bromodeoxyuridine dosing. RNA sequencing of fluorescence-activated cell sorting–purified CRC CAFs was performed to identify a potential therapeutic target in CAFs. To examine the prognostic significance of the stromal target, CRC patient RNA sequencing data and tissue microarray were used. CRC organoids were injected into the colons of knockout mice to assess the mechanism by which the stromal gene contributes to colorectal tumorigenesis. **RESULTS:** Our lineage-tracing studies revealed that in CRC, many ACTA2$^+$ CAFs emerge through proliferation from intestinal pericryptal leptin receptor (*Lepr*)$^+$ cells. These *Lepr*-lineage CAFs, in turn, express melanoma cell adhesion molecule (MCAM), a CRC stroma-specific marker that we identified with the use of RNA sequencing. High MCAM expression induced by transforming growth factor β was inversely associated with patient survival in human CRC. In mice, stromal *Mcam* knockout attenuated orthotopically injected colorectal tumoroid growth and improved survival through decreased tumor-associated macrophage recruitment. Mechanistically, fibroblast MCAM interacted with interleukin-1 receptor 1 to augment nuclear factor κB–IL34/CCL8 signaling that promotes macrophage chemotaxis. **CONCLUSIONS:** In colorectal carcinogenesis, pericryptal *Lepr*-lineage cells proliferate to generate MCAM$^+$ CAFs that shape the tumor-promoting immune microenvironment. Preventing the expansion/differentiation of *Lepr*-lineage CAFs or inhibiting MCAM activity could be effective therapeutic approaches for CRC.

Keywords: Colorectal Cancer; Tumor Microenvironment; Alpha-Smooth Muscle Actin (αSMA); CD146.

WHAT YOU NEED TO KNOW

BACKGROUND AND CONTEXT

Cancer-associated fibroblasts (CAFs) regulate colorectal cancer (CRC) progression. However, the cellular origin of CAFs and how specific CAF lineages contribute to CRC progression are unknown.

NEW FINDINGS

Colonic pericryptal leptin receptor (*LepR*)–lineage cells are a major source of MCAM$^+$ and ACTA2$^+$ CAFs. These MCAM$^+$ CAFs accelerate CRC progression via nuclear factor κB–IL34/CCL8–mediated tumor-associated macrophage recruitment.

LIMITATIONS

This study was performed using mouse models and human tissue samples. Future studies are necessary to assess the therapeutic efficacy of targeting *LEPR*-lineage MCAM$^+$ CAFs in patients with CRC.

IMPACT

Inhibiting proliferation/differentiation of *LEPR*$^+$ cells to MCAM$^+$ CAFs or targeting mature MCAM$^+$ CAFs in established cancer are novel potential therapeutic strategies to treat CRC.

Colorectal cancer (CRC) is a leading cause of cancer-related death. Cancer-associated fibroblasts (CAFs) are histologically prominent and biologically important in CRC initiation, progression, and metastasis.[1] CAFs contribute to carcinogenesis via secretion of growth factors, cytokines, pro-angiogenic factors, and extracellular matrix.[1] Recent studies using immunophenotyping and single-cell RNA sequencing (scRNA-seq) have revealed that CAFs contain heterogeneous subpopulations.[2] It is now apparent that distinct CAF populations have different consequences on cancer growth. Some CAFs promote while others retard cancer growth.[3] The cellular origins of CAFs, whether promoting or retarding, are poorly understood.[1] Regarding the development and consequences of CAFs on CRC growth, there remain at least 3 unresolved questions. First, are CAFs newly generated cells arising through proliferation, or simply old cells acquiring a new phenotype? Second, if any of the CAFs emerge through proliferation, what is their cellular origin? And third, what CAF-derived factors promote cancer progression, and could those be targeted with novel stromal therapies?

Theoretically, CAFs could arise through at least four nonmutually exclusive mechanisms: proliferation, activation, transdifferentiation, and recruitment.[1] Although studies using autochthonous mouse models of cancers have indicated that some CAFs undergo proliferation,[4,5] the relative contribution of proliferating and non-proliferating CAFs to the entire pool remains unclear. Induced by factors such as transforming growth factor (TGF) β,[6] quiescent fibroblasts might undergo phenotypic conversion into activated CAFs: an old cell, but with a new mask (ie, activation). Third, several fate-mapping studies have indicated that nonfibroblast lineage cells, such as epithelial cells, could transdifferentiate into CAFs through epithelial-to-mesenchymal transition (ie, trans-differentiation).[7] Finally, bone marrow transplantation experiments have indicated that about 20% of ACTA2$^+$ (α-smooth muscle actin) CAFs were recruited from the bone

* These authors contributed equally.

Abbreviations used in this paper: **ACTA2, α-smooth muscle actin; AOM, azoxymethane; BrdU, 5-bromodeoxyuridine; CAF, cancer-associated fibroblast; CMS, consensus molecular subtype; CRC, colorectal cancer; DSS, dextran sodium sulfate; FACS, fluorescence-activated cell sorting; Lepr, leptin receptor; MCAM, melanoma cell adhesion molecule; RFP, red fluorescent protein; scRNA-seq, single-cell RNA-sequencing; TAM, tumor-associated macrophage; TCGA, The Cancer Genome Atlas; TGF-β, transforming growth factor β.**

Most current article

0016-5085/$36.00
https://doi.org/10.1053/j.gastro.2021.11.037

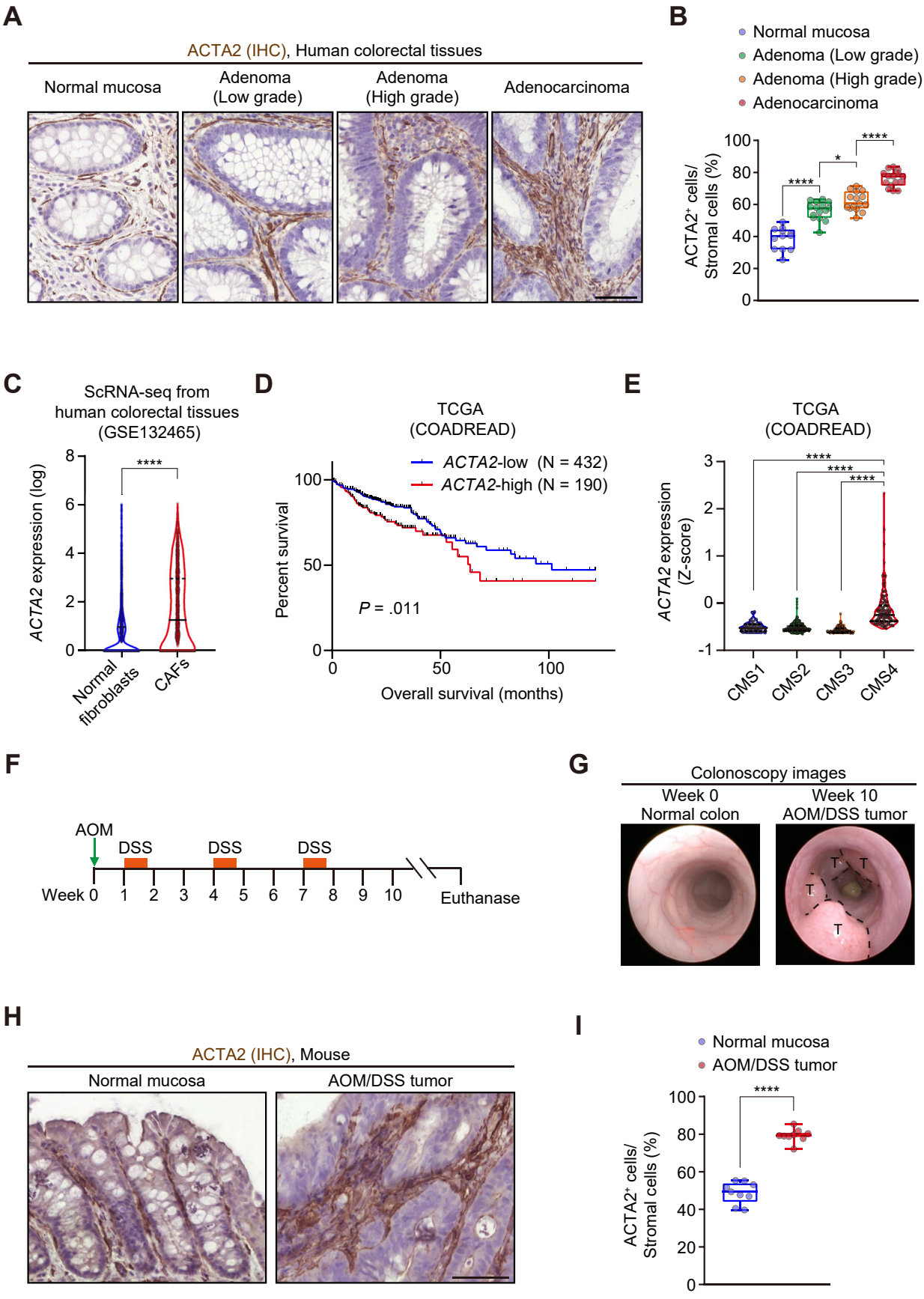
A
ACTA2 (IHC), Human colorectal tissues
Normal mucosa
Adenoma (Low grade)
Adenoma (High grade)
Adenocarcinoma
B
Normal mucosa
Adenoma (Low grade)
Adenoma (High grade)
Adenocarcinoma
ACTA2+ cells/ Stromal cells (%)
C
ScRNA-seq from human colorectal tissues (GSE132465)
ACTA2 expression (log)
Normal fibroblasts
CAFs
D
TCGA (COADREAD)
ACTA2-low (N = 432)
ACTA2-high (N = 190)
Percent survival
P = .011
Overall survival (months)
E
TCGA (COADREAD)
ACTA2 expression (Z-score)
CMS1
CMS2
CMS3
CMS4
F
AOM
DSS
DSS
DSS
Week 0 1 2 3 4 5 6 7 8 9 10
Euthanase
G
Colonoscopy images
Week 0
Normal colon
Week 10
AOM/DSS tumor
H
ACTA2 (IHC), Mouse
Normal mucosa
AOM/DSS tumor
I
Normal mucosa
AOM/DSS tumor
ACTA2+ cells/ Stromal cells (%)

marrow in a mouse model of gastric cancer (ie, recruitment).[8] Human studies have also suggested that bone marrow contribution can be detected in CAFs in several neoplasias, including colorectal.[9] Others, however, have suggested that local precursors were a predominant contributor to ACTA2$^+$ CAFs.[10] Thus, the origin of CAFs remains uncertain. In contrast to fibrosis in organs such as the liver, kidney, and skin, in which the origins of myofibroblasts have been extensively investigated,[11] to our knowledge, no previous CAF studies have comprehensively performed lineage-tracing experiments to track the aforementioned 4 possible CAF sources.

Leptin receptor (*Lepr)* is a well established marker for perivascular mesenchymal cells, which support bone marrow hematopoietic stem cell (HSC) maintenance.[12] Previous fate-mapping studies have demonstrated that *Lepr*-expressing cells give rise to bone and adipocytes formed in the adult normal bone marrow[13] as well as myofibroblasts in primary myelofibrosis.[14] However, the significance of *Lepr*-lineage cells in the development of CAFs is unknown.

Similar to *Lepr*, melanoma cell adhesion molecule (MCAM; also known as CD146 and MUC18) is highly expressed by perivascular stromal cells in the bone marrow and has been suggested to be important in the HSC niche.[15] MCAM is also expressed by endothelial cells, melanoma cells, pericytes, and CAFs.[16,17] MCAM expressed in endothelial and melanoma cells contributes to cancer progression by promoting cancer cell growth, angiogenesis, and metastasis.[17,18] Recently, scRNA-seq analyses have revealed that *MCAM* defines a subset of pericyte-like CAFs that secrete tumor-promoting immunomodulatory cytokines in human cholangiocarcinoma and breast cancer.[19,20] The biological role of MCAM$^+$ CAFs, however, has been poorly defined in CRC.

This study, for the first time, comprehensively addresses the cellular origins, dynamics, and consequences of specific CAFs in CRC. Using lineage tracing, we identify intestinal pericryptal *Lepr*-lineage cells as a major source of proliferating CAFs in a mouse model of CRC. Next, by combining fluorescence-activated cell sorting (FACS), RNA-seq, and immunohistochemistry, we show these CAFs express MCAM. We investigate the clinical significance of MCAM expression with the use of RNA-seq data and tissue microarray from human CRC samples. Finally, we uncover the mechanism of stromal MCAM action in CRC with the use of newly generated *Mcam*-null mice and mouse colonoscopy.

Materials and Methods

Statistical Analysis

Comparison of 2 groups was performed using 2-tailed unpaired *t* tests or Mann-Whitney *U* tests. For multiple comparisons, we used analysis of variance or Kruskal-Wallis test. For survival analyses, Kaplan-Meier survival estimation with a log-rank (Mantel-Cox) test was performed. Statistical analyses were conducted with the use of GraphPad Prism 8.00 or SPSS Statistics 25. *P* values of <0.05 were considered to be statistically significant.

For all other materials and methods, see the Supplementary Materials.

Results

Desmoplasia Is Increased During Colorectal Carcinogenesis in Humans and Mice

To explore whether desmoplasia is increased during colorectal carcinogenesis and to identify a suitable mouse model to investigate this, we performed immunohistochemistry for ACTA2, a well established marker for CAFs, in human colorectal samples. The ratio of ACTA2$^+$ fibroblasts in the total stromal cells increased from normal to low-grade adenoma to high-grade adenoma, and ultimately adenocarcinoma (Figure 1*A* and *B*). The elevated ACTA2 expression level during colorectal carcinogenesis was corroborated by an analysis of expression microarray data from human colorectal tissues (Supplementary Figure 1*A*). Analyses of scRNA-seq data from human CRC tissues[2] also demonstrated that *ACTA2* expression is increased in CAFs compared with normal fibroblasts, with the highest *ACTA2* transcripts observed in pericytes among various CAF subpopulations (Figure 1*C*; Supplementary Figure 1*B* and *C*).

Next, we investigated the prognostic significance of *ACTA2* expression in The Cancer Genome Atlas (TCGA) data. High *ACTA2* expression was inversely associated with overall survival in patients with CRC (Figure 1*D*). High *ACTA2* expression, as well as high expression of *FAP*, an

Figure 1. ACTA2 expression is increased during colorectal carcinogenesis in humans and mice. (*A*, *B*) Immunohistochemistry (IHC) for ACTA2 in human colorectal samples. (*A*) Representative pictures. (*B*) ACTA2 positivity in total stromal cells (visualized by hematoxylin counterstaining). Three HPFs (×400)/patient, 4–5 patients each. (*C*) Violin plots depict *ACTA2* transcripts in normal fibroblasts (n = 2053 cells) and CRC CAFs (n = 1854 cells) assessed by means of single-cell RNA sequencing (scRNA-seq) from human colorectal tissues. (*D*) Kaplan-Meier survival curves in The Cancer Genome Atlas (TCGA) data set. (*E*) Violin plots showing *ACTA2* expression level in 4 consensus molecular subtypes (CMSs). n = 76, 220, 72, and 143 patients (CMS1–4). (*F*) Scheme for the experimental course of azoxymethane (AOM)/dextran sulfate sodium (DSS)–induced colorectal carcinogenesis. (*G*) Representative endoscopic images of the normal colon mucosa and AOM/DSS tumors. T, tumor. (*H, I*) Immunohistochemistry for ACTA2 in the normal mucosa and AOM/DSS tumors. (*H*) Representative pictures. (*I*) ACTA2 positivity in total stromal cells. 3 HPFs/mouse, 3 mice each. One-way analysis of variance followed by Tukey's post hoc multiple comparison test (*B*), Wilcoxon rank-sum test (*C*), log-rank test (*D*), Kruskal-Wallis test followed by Dunn's multiple comparisons test (*E*), and 2-tailed unpaired Student *t* test (*I*): ****$P < 0.0001$; *$P = 0.0451$. Scale bars, 50 μm. Box plots have whiskers of maximum and minimum values; the boxes represent interquartile range and median. In violin plots, solid and dotted black lines denote median and quartiles, respectively. ACTA2, α-smooth muscle actin; AOM, azoxymethane; CAF, cancer-associated fibroblast ; CRC, colorectal cancer; DSS, dextran sulfate sodium; HPF, high-power field.

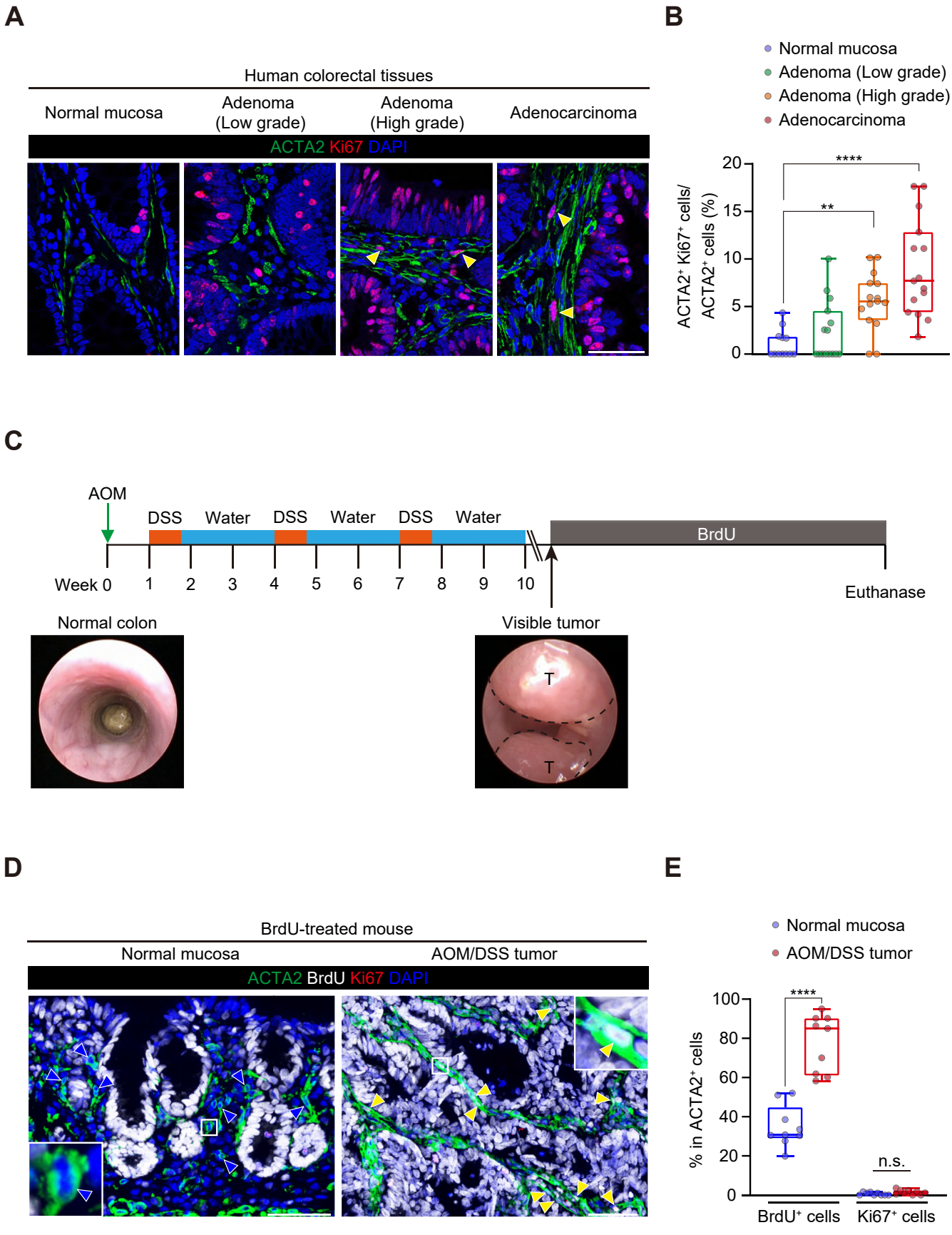
A
Human colorectal tissues
Normal mucosa
Adenoma (Low grade)
Adenoma (High grade)
Adenocarcinoma
ACTA2 Ki67 DAPI
B
Normal mucosa
Adenoma (Low grade)
Adenoma (High grade)
Adenocarcinoma
ACTA2+ Ki67+ cells/ ACTA2+ cells (%)
20
15
10
5
0
****
**
C
AOM
DSS
Water
DSS
Water
DSS
Water
BrdU
Week 0
1
2
3
4
5
6
7
8
9
10
Euthanase
Normal colon
Visible tumor
T
T
D
BrdU-treated mouse
Normal mucosa
AOM/DSS tumor
ACTA2 BrdU Ki67 DAPI
E
Normal mucosa
AOM/DSS tumor
% in ACTA2+ cells
100
80
60
40
20
0
****
n.s.
BrdU+ cells
Ki67+ cells

activated fibroblast marker,[1] was consistently associated with poor prognosis across multiple expression datasets from CRC patients (Supplementary Figure 2). The highest *ACTA2* expression was observed in the poor-prognosis stroma-rich molecular subtype of CRC (consensus molecular subtype [CMS] 4)[21] (Figure 1*E*).

We then sought to explore whether ACTA2$^+$ fibroblasts are similarly increased in mouse models of CRC. To this end, we performed ACTA2 immunohistochemistry with the use of tumors from the azoxymethane (AOM)/dextran sulfate sodium (DSS) (Figure 1*F* and *G*) and *Apc*$^{Min/+}$ mouse models. In line with a previous study,[22] ACTA2 expression was significantly elevated in the stroma of AOM/DSS tumors compared with the adjacent normal mucosa (Figure 1*H* and *I*). Similarly, small intestinal tumors from *Apc*$^{Min/+}$ mice showed an increase in stromal ACTA2 expression compared with the adjacent normal tissue, but to a lesser extent than the AOM/DSS mouse model (Supplementary Figure 3). Taken together, these data suggest that *ACTA2*$^+$ fibroblast number increases throughout colorectal carcinogenesis in humans, and this is recapitulated in the AOM/DSS mouse model of CRC.

A Subpopulation of CRC CAFs Arises Through Proliferation in Humans and Mice

We next addressed the question of whether CAFs emerge through cell division or simply increase ACTA2 expression in existing cells. Co-staining for ACTA2 and Ki67 with the use of human colorectal samples revealed that the percentage of ACTA2 and Ki67 double-positive cells (ie, proliferating ACTA2$^+$ CAFs) was increased in high-grade adenoma and adenocarcinoma compared with normal colorectal mucosa, with about 10% of ACTA2$^+$ CAFs marked by Ki67 in adenocarcinoma (Figure 2*A* and *B*). Analysis of scRNA-seq data from human CRC and normal mucosa[2] confirmed that a subcluster of *ACTA2*$^+$ CAFs expressed *MKI67*, and this co-expressing population was not found in fibroblasts from the normal mucosa (Supplementary Figure 4). These data suggest that human CRC CAFs undergo mitosis during malignant progression.

Ki67 only temporarily marks actively cycling cells, so our analysis of proliferation of human CRC CAFs may underestimate CAFs that divided at an earlier time point. To capture the entire population of CAFs that underwent proliferation during carcinogenesis, we took advantage of continuous 5-bromodeoxyuridine (BrdU) labeling in the AOM/DSS mouse model. After the last course of DSS/water treatment (5-day DSS treatment followed by a 16-day recovery period with normal drinking water), BrdU dosing commenced at the onset of observable tumors (Figure 2*C*). The ratio of ACTA2$^+$ fibroblasts that incorporated BrdU was significantly elevated in AOM/DSS tumors compared with the adjacent nonneoplastic colon, with approximately 75% of ACTA2$^+$ fibroblasts in AOM/DSS tumors marked by BrdU (Figure 2*D* and *E*; Supplementary Figure 5). Colonoscopic and microscopic evaluation of AOM/DSS tumors confirmed the absence of excavated ulcers or severe inflammation at the time point when BrdU labeling started (Figure 2*C*; Supplementary Figure 6). These data indicate that ACTA2$^+$ fibroblasts have divided during AOM/DSS tumorigenesis, after DSS-induced acute colitis subsided. Contrasting with the BrdU incorporation ratio, the ratio of actively proliferating fibroblasts (Ki67$^+$ACTA2$^+$ fibroblasts) in the total pool of ACTA2$^+$ fibroblasts was only about 1.5% in AOM/DSS tumors and was not significantly different from the ratio of proliferating fibroblasts in the normal mouse colorectal mucosa (Figure 2*D* and *E*). Collectively, our data suggest that, in AOM/DSS tumors, the majority of ACTA2$^+$ fibroblasts at humane end point were in quiescent G0 phase as evaluated by Ki67 negativity, but approximately three-fourths of the fibroblasts had undergone cell division and incorporated BrdU during colitis-associated tumorigenesis after the last DSS/recovery cycle.

Lepr-*Lineage Stromal Cells Are a Major Contributor to the Proliferating Fibroblasts in AOM/DSS CRC*

We next sought to establish the cellular origin of the proliferating fibroblasts in AOM/DSS tumors by using a lineage-tracing strategy. We selected transgenic mouse lines that 1) identified putative colorectal mesenchymal stem-progenitor cells (*Lepr*-Cre; Rosa26-LSL-tdtomato,[12] *Grem1*-CreERT2; Rosa26-LSL-ZsGreen[23] and *Islr*-CreERT2; Rosa26-LSL-tdtomato[3]), 2) labeled epithelium (*Krt19*-Cre; Rosa26-mt/mG), or 3) marked bone marrow–derived cells through a combination of bone marrow from *Acta2*–red fluorescent protein (RFP) mouse transplanted into non-RFP recipients (Figure 3). These fate-mapping experiments were coupled with BrdU labeling beginning at the onset of observable tumors after the last DSS/recovery cycle (Figure 2*C*). Tamoxifen was administered to the inducible Cre lines at postnatal day 6.

Immunofluorescence for EPCAM, a pan-epithelial cell marker, showed that all *Lepr*-, *Grem1*-, and *Islr*-lineage cells were observed only within the EPCAM$^-$ stroma, validating

Figure 2. A subset of ACTA2$^+$ CAFs proliferate during colorectal carcinogenesis in humans and mice. (*A, B*) Co-immunofluorescence for ACTA2 and Ki67 in human colorectal samples. (*A*) Representative pictures. *Yellow arrowheads* denote proliferating CAFs (ACTA2$^+$Ki67$^+$ cells). (*B*) Ki67 positivity in total ACTA2$^+$ cells. Three HPFs (×400)/patient, 4–5 patients each. (*C*) Scheme for the experimental course of AOM/DSS-induced colon carcinogenesis and BrdU administration. After the end of the last DSS/water cycle, continuous BrdU administration was commenced once a visible tumor was observed via mouse colonoscopy. T, tumor. (*D, E*) Co-immunofluorescence for ACTA2, BrdU, and Ki67 in the normal colon mucosa and AOM/DSS tumors. (*D*) Representative images. *Blue and yellow arrowheads* denote ACTA2$^+$BrdU$^-$ and ACTA2$^+$BrdU$^+$ cells, respectively. (*E*) BrdU positivity (*left*) and Ki67 positivity (*right*) in total ACTA2$^+$ cells. 3 HPFs/mouse, 3 mice each. Kruskal-Wallis test followed by Dunn's multiple comparisons test (*B*) and 2-tailed unpaired Student *t* test (*E*): ****$P < 0.0001$; **$P = 0.0077$; ns, $P = 0.0857$. Scale bars, 50 μm. BrdU, 5-bromodeoxyuridine; other abbreviations as in Figure 1.

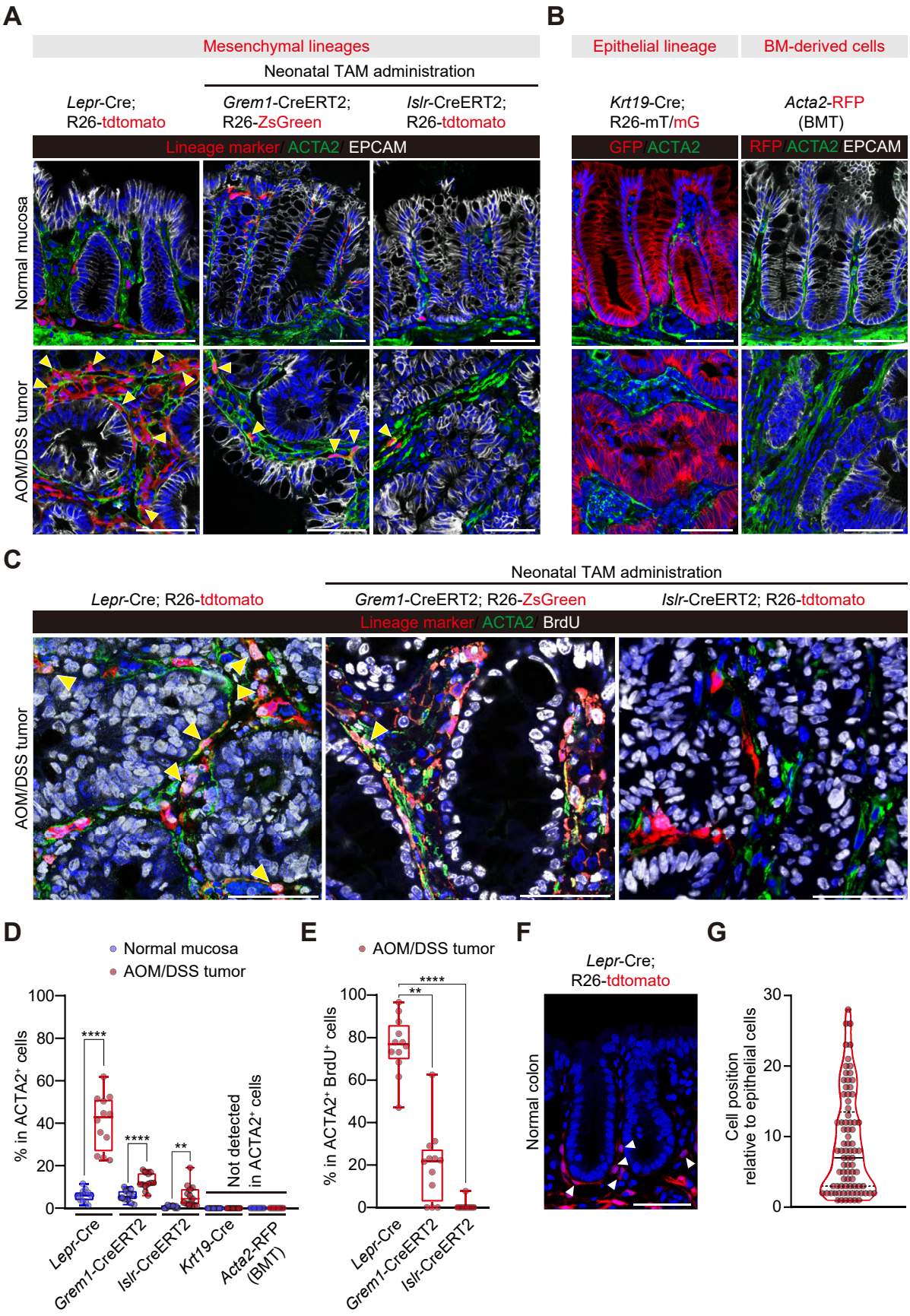
A
Mesenchymal lineages
Neonatal TAM administration
Lepr-Cre; R26-tdtomato
Grem1-CreERT2; R26-ZsGreen
Islr-CreERT2; R26-tdtomato
Lineage marker/ ACTA2/ EPCAM
Normal mucosa
AOM/DSS tumor
B
Epithelial lineage
BM-derived cells
Krt19-Cre; R26-mT/mG
Acta2-RFP (BMT)
GFP/ACTA2
RFP/ACTA2/ EPCAM
C
Neonatal TAM administration
Lepr-Cre; R26-tdtomato
Grem1-CreERT2; R26-ZsGreen
Islr-CreERT2; R26-tdtomato
Lineage marker/ ACTA2/ BrdU
AOM/DSS tumor
D
Normal mucosa
AOM/DSS tumor
% in ACTA2+ cells
Not detected in ACTA2+ cells
Lepr-Cre
Grem1-CreERT2
Islr-CreERT2
Krt19-Cre
Acta2-RFP (BMT)
E
AOM/DSS tumor
% in ACTA2+ BrdU+ cells
F
Lepr-Cre; R26-tdtomato
Normal colon
G
Cell position relative to epithelial cells

their mesenchymal identity (Figure 3*A*). In AOM/DSS tumors, approximately one-half of ACTA2$^+$ fibroblasts and 75% of proliferating BrdU$^+$ACTA2$^+$ fibroblasts were *Lepr*-lineage-positive, with a smaller proportion of ACTA2$^+$ fibroblasts derived from the *Grem1*-lineage and *Islr*-lineage (Figure 3*A* and *C*–*E*). *Lepr*-lineage cells represented about 47.1% and 17.4% of the total PDGFRA$^+$ fibroblasts in the AOM/DSS tumors and normal colons, respectively (Supplementary Figure 7). Together, these results suggest that *Lepr*-lineage stromal cells are a major source of proliferating ACTA2$^+$ fibroblasts during AOM/DSS carcinogenesis.

Lepr-*Lineage Cells Contribute to ACTA2$^+$ Proliferating CAFs in a CRC Organoid Transplantation Model*

We next asked whether *Lepr*-lineage cells also give rise to proliferating ACTA2$^+$ CAFs in a distinct model of CRC. To this end, we colonoscopically injected *Apc*$^{\Delta/\Delta}$, *Kras*$^{G12D/\Delta}$, *Trp53*$^{\Delta/\Delta}$ mouse CRC organoids (hereafter termed AKP tumoroids) into the colons of *Lepr*-Cre; Rosa26-LSL-tdtomato mice (Supplementary Figures 8 and 9*A*). Continuous BrdU dosing commenced 1 day after tumoroid transplantation. In this model, approximately 72% of ACTA2$^+$ CAFs underwent proliferation as assessed by BrdU positivity (Supplementary Figure 9*B* and *C*). Similarly to our findings with the AOM/DSS model, *Lepr*-lineage cells were a major contributor to BrdU$^+$ACTA2$^+$ CAFs in this model, with 53% of the proliferating CAFs derived from *Lepr* lineage (Supplementary Figure 9*B*–*E*). Our *Lepr*-lineage tracing data from colitis-associated and sporadic CRC models suggest that the majority of proliferating ACTA2$^+$ CAFs in CRC originate from *Lepr*-lineage cells.

Neither Epithelium nor Bone Marrow Recruitment Contributed to ACTA2$^+$ CAFs in the AOM/DSS Mouse Model of CRC

We explored whether colonic epithelial cells could undergo epithelial-mesenchymal transition into colorectal CAFs. For this purpose, we used constitutive *Krt19*-Cre; Rosa26-mt/mG mice to track the fate of *Krt19*-lineage colonic epithelial cells. All colonic cells with epithelial morphology were marked after reporter recombination by Cre recombinase driven by the *Krt19* promoter (Figure 3*B*). However, no *Krt19*-lineage cells were positive for ACTA2 in either normal colon or AOM/DSS tumors (Figure 3*B* and *D*). This suggests that, at least in this mouse model of CRC, the epithelium is not a source of ACTA2$^+$ CAFs.

Next, to assess the contribution of bone marrow–derived cells to the AOM/DSS tumor stroma, we performed bone marrow transplantation experiments with the use of an *Acta2*-RFP reporter mouse as a donor. Initially, we validated that, in *Acta2*-RFP mice that did not undergo bone marrow transplantation, RFP was expressed by fibroblastic cells in AOM/DSS tumors, confirming that the *Acta2* promoter is active in this CRC mouse model (Supplementary Figure 10). To perform bone marrow transplantation from *Acta2*-RFP mice, wild-type recipient mice were subjected to total body irradiation and transplanted with whole bone marrow cells from *Acta2*-RFP donor mice. Then, the mice were treated with AOM/DSS to induce colorectal tumors (Supplementary Figure 11*A*). Quantitative polymerase chain reaction for RFP with the use of genomic DNA isolated from the bone marrow of the recipient mice confirmed engraftment of RFP$^+$ cells in the recipient bone marrow (Supplementary Figure 11*B*). Transplanted *Acta2*-RFP$^+$ cells were also observed in the small intestine of the wild-type recipients, further validating the engraftment (Supplementary Figure 11*C*). However, no bone marrow–transplanted RFP$^+$ cells were observed in AOM/DSS tumors in wild-type recipient mice (Figure 3*B* and *D*). This indicates that, at least in this experimental CRC model, CAFs did not arise via recruitment from the bone marrow, but only from local precursors.

Collectively, our data with 5 distinct genetically engineered mouse models suggest that tissue-resident *Lepr*-lineage stromal cells are a key contributor to the ACTA2$^+$ CAFs in AOM/DSS tumors.

Lepr-*Lineage Intestinal Stromal Cells Undergo Proliferation and Differentiation Into ACTA2$^+$ CAFs During AOM/DSS Carcinogenesis*

We next sought to characterize *Lepr*-lineage cells in the normal colon and AOM/DSS tumors. In the normal colonic mucosa, pericryptal *Lepr*-lineage cells were preferentially located near the base of the crypts (Figure 3*F* and *G*). *Lepr*-

Figure 3. Proliferating ACTA2$^+$ fibroblasts in AOM/DSS tumors derive predominantly from *Lepr*-lineage cells. (*A*) Immunofluorescence for ACTA2 and EPCAM (a pan-epithelial cell marker) in the normal colon mucosa and AOM/DSS tumors with the use of fate-mapping mouse models. *Yellow arrowheads* denote lineage-marker$^+$ACTA2$^+$ cells. See (*D*) for quantification. R26, Rosa26-loxP-stop-loxP; BM, bone marrow; BMT, bone marrow transplantation; GFP, green fluorescent protein; RFP, red fluorescent protein; TAM, tamoxifen. (*B*) Immunofluorescence for ACTA2 in the normal mucosa and AOM/DSS tumors in *Krt19*-Cre mice (*left*). Immunofluorescence for ACTA2 and EPCAM in the normal mucosa and AOM/DSS tumor, in a wild-type recipient mouse transplanted with bone marrow cells from an *Acta2*-RFP mouse (*right*). (*C*) Immunofluorescence for ACTA2 and BrdU in AOM/DSS tumors in the BrdU-treated fate-mapping mouse models. *Yellow arrowheads* denote proliferating CAFs that were derived from each cellular lineage (lineage-marker$^+$ACTA2$^+$BrdU$^+$ cells). (*D*) The ratios of lineage-marker$^+$ cells in total ACTA2$^+$ cells. 4 HPFs/mouse. n = 3 mice (*Lepr*-Cre, *Grem1*-CreERT2, *Islr*-CreERT2, *Acta2*-RFP) and n = 2 mice (*Krt19*-Cre). (*E*) The ratios of lineage marker$^+$ cells in total proliferating CAFs. 4 HPFs/mouse. 3 mice each. (*F, G*) Cellular positions of *Lepr*-lineage stromal cells in the normal adult mouse colon. (*F*) Representative pictures. White arrowheads denote *Lepr*-lineage tdtomato$^+$ cells. (*G*) Violin plots showing the positions of pericryptal *Lepr*-lineage stromal cells relative to the adjacent epithelial position. n = 81 *Lepr*-lineage cells from 3 mice. Scale bars, 50 μm. Two-tailed unpaired *t* test with Welch's correction (*D*) and Kruskal-Wallis test followed by Dunn's multiple comparisons test (*E*): ****$P < 0.0001$; **$P = 0.0030$ (*D*); **$P = 0.0043$ (*E*). Lepr, leptin receptor; other abbreviations as in Figures 1 and 2.

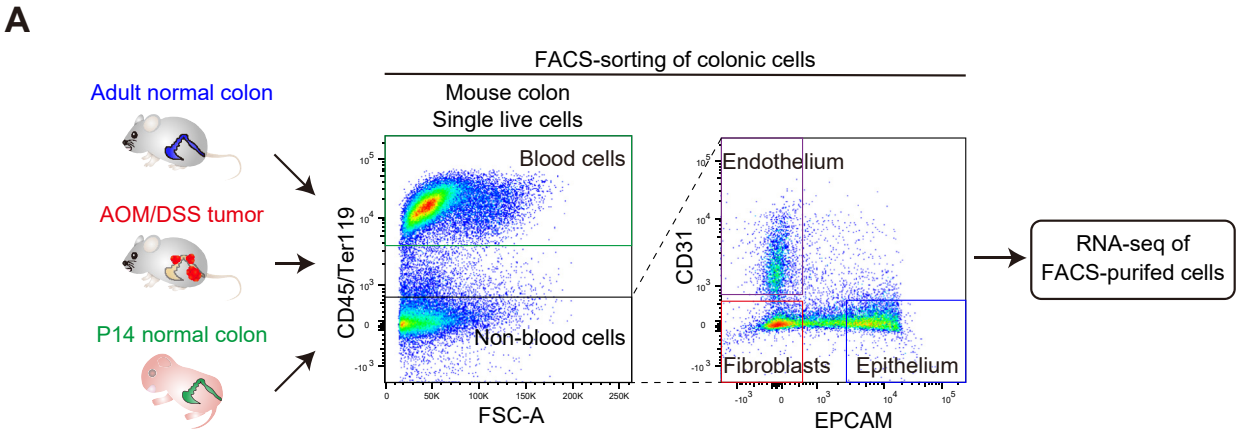
A
FACS-sorting of colonic cells
Adult normal colon
AOM/DSS tumor
P14 normal colon
Mouse colon
Single live cells
Blood cells
Non-blood cells
CD45/Ter119
FSC-A
Endothelium
Fibroblasts
Epithelium
CD31
EPCAM
RNA-seq of FACS-purifed cells

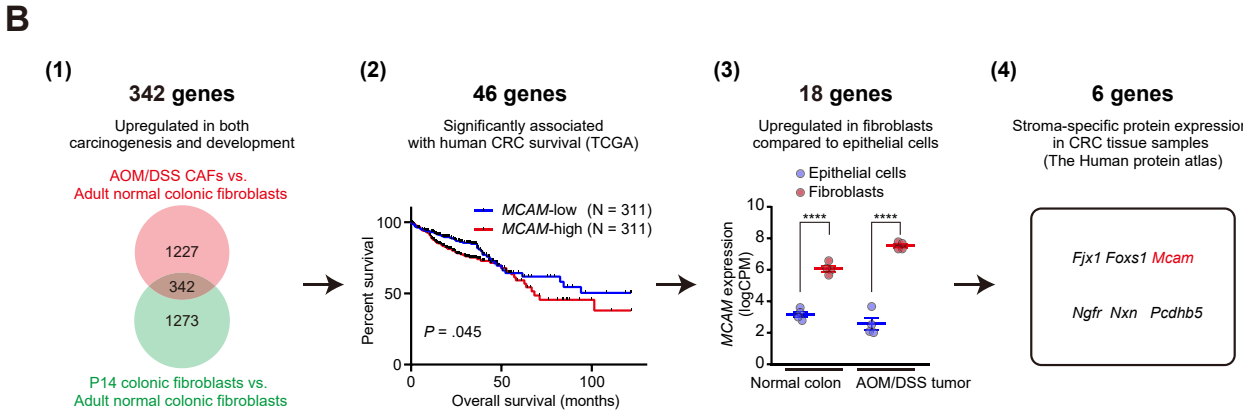
B
(1)
342 genes
Upregulated in both carcinogenesis and development
AOM/DSS CAFs vs. Adult normal colonic fibroblasts
1227
342
1273
P14 colonic fibroblasts vs. Adult normal colonic fibroblasts
(2)
46 genes
Significantly associated with human CRC survival (TCGA)
MCAM-low (N = 311)
MCAM-high (N = 311)
Percent survival
P = .045
Overall survival (months)
(3)
18 genes
Upregulated in fibroblasts compared to epithelial cells
Epithelial cells
Fibroblasts
MCAM expression (logCPM)
Normal colon
AOM/DSS tumor
(4)
6 genes
Stroma-specific protein expression in CRC tissue samples (The Human protein atlas)
Fjx1 Foxs1 Mcam
Ngfr Nxn Pcdhb5

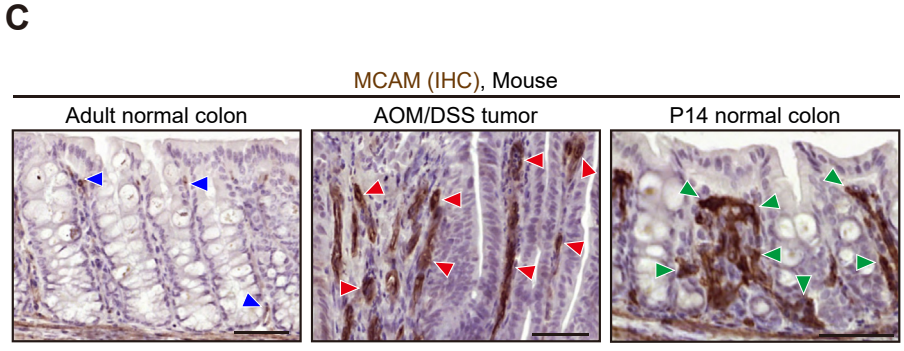
C
MCAM (IHC), Mouse
Adult normal colon
AOM/DSS tumor
P14 normal colon

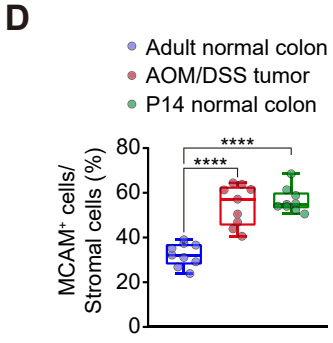
D
Adult normal colon
AOM/DSS tumor
P14 normal colon
MCAM+ cells/ Stromal cells (%)

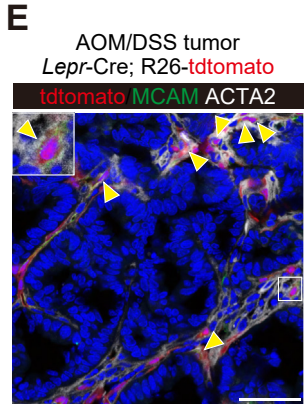
E
AOM/DSS tumor
Lepr-Cre; R26-tdtomato
tdtomato MCAM ACTA2

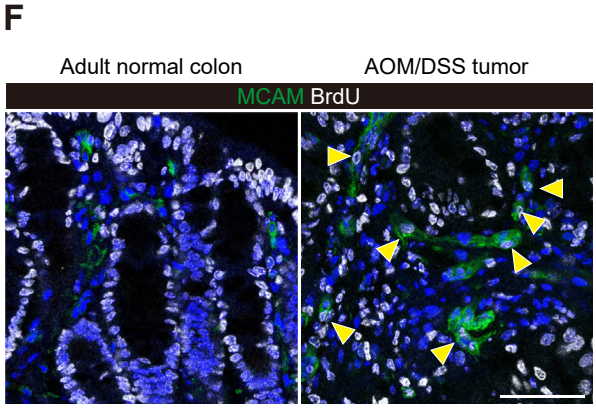
F
Adult normal colon
AOM/DSS tumor
MCAM BrdU

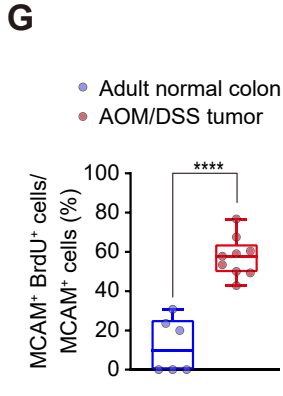
G
Adult normal colon
AOM/DSS tumor
MCAM+ BrdU+ cells/ MCAM+ cells (%)

lineage stromal cells in AOM/DSS tumors exhibited higher ACTA2 positivity than *Lepr*-lineage stromal cells in the normal mucosa, indicating that *Lepr*-lineage cells underwent phenotypic conversion into ACTA2$^+$ CAFs during carcinogenesis (Supplementary Figure 12*A* and *B*). BrdU labeling in AOM/DSS-treated mice revealed that *Lepr*-lineage cells showed higher proliferation in AOM/DSS tumors compared with the adjacent normal mucosa (Supplementary Figure 12*C* and *D*). Single-molecule fluorescent RNA in situ hybridization for *Lepr* revealed that active expression of *Lepr* in *Lepr*-lineage cells was reduced in the AOM/DSS tumor compared with the normal colon (Supplementary Figure 12*E* and *F*). Together, these findings indicate that intestinal *Lepr*-lineage stromal cells undergo expansion and differentiation to ACTA2$^+$ myofibroblasts at the expense of *Lepr* expression during AOM/DSS colorectal carcinogenesis.

Identification of MCAM as a CRC Stroma-Specific Marker That Defines a Subset of Lepr-Lineage Proliferating CAFs.

Lower *Lepr* expression in the CRC mesenchyme could potentially make it challenging to therapeutically target *Lepr*-lineage CAFs based on active *Lepr* expression in established cancers. Therefore, we next aimed to identify a stromal factor that is actively expressed in the CRC mesenchyme as a potential therapeutic stromal target to treat CRC.

As a strategy to identify the most biologically relevant stromal targets, we were inspired by the parallels between cancer and developmental biology.[24,25] For example, factors involved in fibroblast activation (eg, TGF-β) and inflammation (eg, nuclear factor (NF) κB) play crucial roles in both carcinogenesis and organ development.[1,25,26] Therefore, we decided to triangulate the fibroblastic factors that were significantly up-regulated in both tumorigenesis and development compared to adult colonic fibroblasts.

We first sorted fibroblasts using a negative selection strategy. Fibroblasts were selected based on their lack of expression of blood cell markers (CD45 and Ter119), an endothelial marker (CD31), and an epithelial marker (EPCAM) from AOM/DSS tumors, developmental colon (postnatal day 14), and normal adult colon (Figure 4*A*). Fibroblast markers such as *Grem1*, *Acta2*, and *Fap* were highly expressed in the FACS-sorted mesenchymal cells (CD45$^-$, Ter119$^-$, CD31$^-$, EPCAM$^-$), validating their enrichment for fibroblasts (Supplementary Figure 13). RNA-seq from the FACS-purified fibroblasts revealed that 342 genes were differentially up-regulated in both the AOM/DSS tumors and the early postnatal colons compared with the normal adult colon fibroblasts (Figure 4*B*, step 1). Next, we analyzed the prognostic significance of these 342 genes by performing survival analysis with the use of TCGA data, resulting in the selection of 46 genes that were associated with human CRC survival (Figure 4*B*, step 2; Supplementary Table 1). Next, to focus on stroma-specific targets, using our RNA-seq data from normal adult colon and AOM/DSS tumors, we selected 18 stroma-specific genes that were up-regulated in fibroblasts compared with epithelial cells (Figure 4*B*, step 3; Supplementary Table 1). Then, to examine for genes expressed at the protein level in human CRC stroma, we interrogated human CRC immunohistochemistry data in the Human Protein Atlas database and selected 6 proteins that were highly expressed in the CRC stroma (Figure 4*B*, step 4; Supplementary Figure 14). Finally, our immunohistochemistry data for candidate genes showed that MCAM was the only candidate that was consistently up-regulated in the stroma of AOM/DSS tumors and the developmental colon compared with the normal adult colon (Figure 4*C* and *D*; Supplementary Figure 15).

Next, we explored the stromal MCAM expression in human and mouse colorectal tissues. Analyses of scRNA-seq from human CRC tissues[2] and ulcerative colitis samples revealed that the high *MCAM* expression was observed in pericytes compared with other cell subpopulations such as endothelial cells, epithelial cells, and immune cells (Supplementary Figure 16*A* and *B*). In AOM/DSS tumors, co-immunofluorescence for CD31, ACTA2, CD45, and EPCAM showed that approximately 45% of MCAM$^+$ cells expressed

Figure 4. Identification of MCAM as a CRC mesenchyme–specific marker that represents a subset of *Lepr*-lineage proliferating cells. (*A*) Experimental schematic for isolating colonic fibroblasts from the normal adult colon, AOM/DSS tumors, and postnatal day 14 colon. Gating strategy to isolate CD45$^-$Ter119$^-$CD31$^-$EPCAM$^-$ fibroblasts by fluorescence-activated cell-sorting (FACS) is shown for 1 mouse adult normal colon. n = 4 mice each. (*B*) Strategy to identify a colonic stromal gene up-regulated in development and carcinogenesis, which is associated with human CRC survival. (*1*) Venn diagram showing 342 genes up-regulated in AOM/DSS tumors and postnatal day 14 colon compared with normal adult colon fibroblasts. (*2*) Survival analysis using The Cancer Genome Atlas (TCGA) data set. (*3*) Using our RNA sequencing data, genes up-regulated in EPCAM$^-$CD31$^-$CD45$^-$Ter119$^-$ fibroblasts compared with EPCAM$^+$ epithelial cells, in both normal adult colon and AOM/DSS tumors, were selected. Mean ± SEM. (*4*) The Human Protein Atlas data were used to select genes whose protein expression was restricted to the CRC stroma. *Mcam* is highlighted in *red*. (*C, D*) Immunohistochemistry (IHC) for MCAM. (*C*) Representative images. *Blue, red, and green arrowheads* denote MCAM expression in the normal adult colon, AOM/DSS tumor, and postnatal day 14 colon, respectively. (*D*) The ratios of MCAM$^+$ cells in total stromal cells (visualized by means of hematoxylin counterstaining). 3 HPFs/mouse, 3 mice each. (*E*) Co-Immunofluorescence for MCAM and ACTA2 with the use of AOM/DSS tumors from *Lepr*-Cre; Rosa26-tdtomato mice. *Yellow arrowheads* denote *Lepr*-lineage MCAM$^+$ ACTA2$^+$ CAFs. See Supplementary Figure 17*C* and *D* for quantification and separate channel images. (*F, G*) Co-immunofluorescence for MCAM and BrdU. (*F*) Representative images. *Yellow arrowheads* denote proliferating MCAM$^+$ cells. (*G*) The ratio of MCAM$^+$BrdU$^+$ cells in total MCAM$^+$ cells. 3 HPFs/mouse, 2–3 mice each. Scale bars, 50 μm. Log-rank test (B(*2*)), 1-way analysis of variance followed by Tukey's post hoc multiple comparison test (*B*(*3*) and *D*), and 2-tailed unpaired Student *t* test (*G*): ****$P < 0.0001$. MCAM, melanoma cell adhesion molecule; other abbreviations as in Figures 1–3.

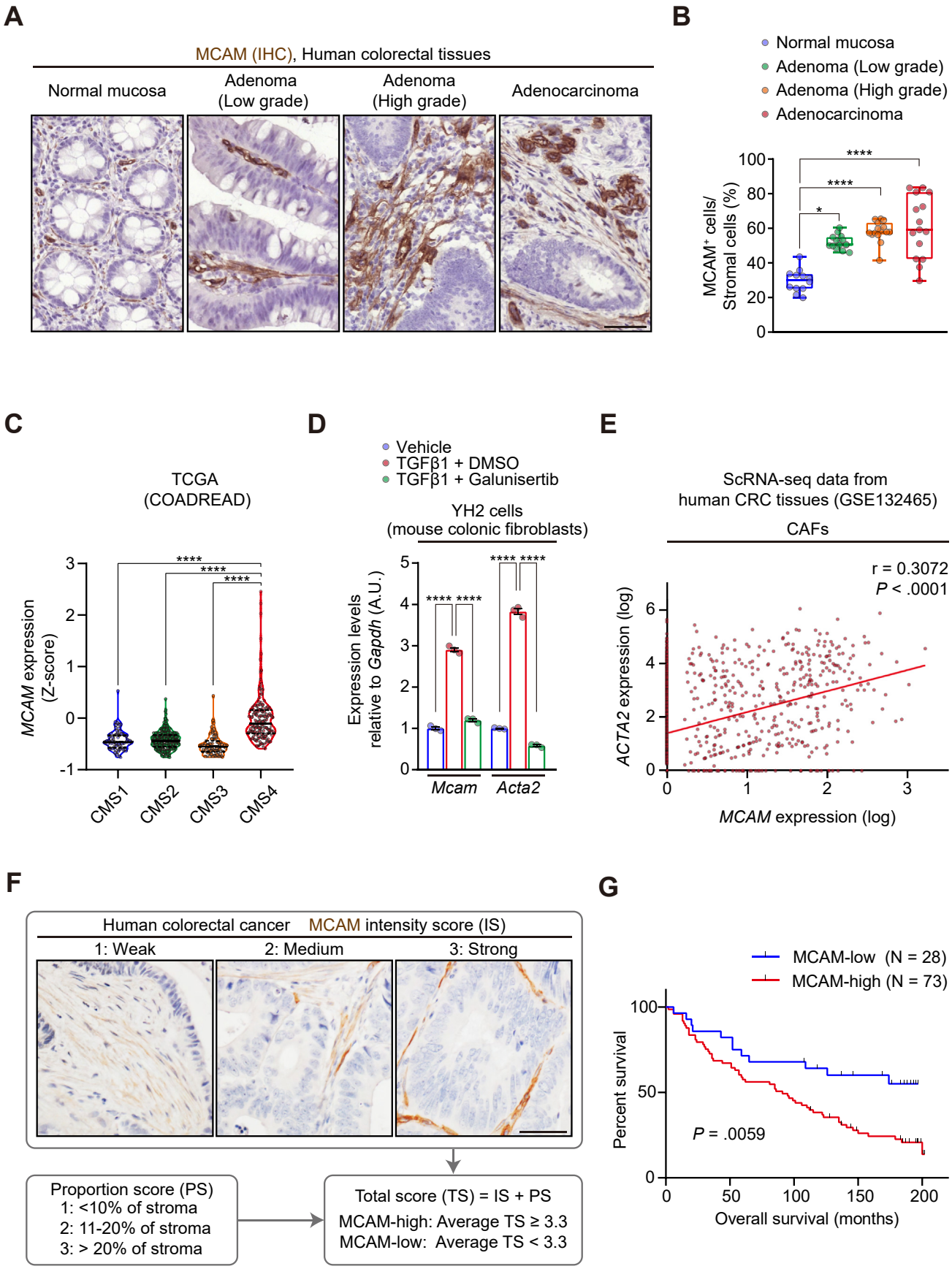
A
MCAM (IHC), Human colorectal tissues
Normal mucosa
Adenoma (Low grade)
Adenoma (High grade)
Adenocarcinoma
B
Normal mucosa
Adenoma (Low grade)
Adenoma (High grade)
Adenocarcinoma
MCAM+ cells/ Stromal cells (%)
C
TCGA (COADREAD)
MCAM expression (Z-score)
CMS1
CMS2
CMS3
CMS4
D
Vehicle
TGFβ1 + DMSO
TGFβ1 + Galunisertib
YH2 cells (mouse colonic fibroblasts)
Expression levels relative to Gapdh (A.U.)
Mcam
Acta2
E
ScRNA-seq data from human CRC tissues (GSE132465)
CAFs
r = 0.3072
P < .0001
ACTA2 expression (log)
MCAM expression (log)
F
Human colorectal cancer MCAM intensity score (IS)
1: Weak
2: Medium
3: Strong
Proportion score (PS)
1: <10% of stroma
2: 11-20% of stroma
3: > 20% of stroma
Total score (TS) = IS + PS
MCAM-high: Average TS ≥ 3.3
MCAM-low: Average TS < 3.3
G
MCAM-low (N = 28)
MCAM-high (N = 73)
Percent survival
P = .0059
Overall survival (months)

a pericyte/CAF marker, ACTA2 (Supplementary Figure 16*C* and *D*).

To characterize the cellular sources of MCAM$^+$ CAFs in CRC, we performed immunofluorescence for MCAM in the 3 mesenchymal fate-mapping mouse models (*Lepr*-Cre, *Grem1*-CreERT2, and *Islr*-CreERT2 mice). Our data revealed that about 80% of MCAM$^+$ACTA2$^+$ CAFs were derived from the *Lepr* lineage in AOM/DSS tumors (Figure 4*E*; Supplementary Figure 17). We also co-stained MCAM and BrdU in AOM/DSS-treated mice that were administered BrdU during carcinogenesis. In keeping with previous scRNA-seq data showing that *Mcam* was highly expressed by a proliferative subpopulation of CAFs,[5] more than half of the MCAM$^+$ cells were positive for BrdU, indicating that the majority of MCAM$^+$ cells arose through proliferation (Figure 4*F* and *G*). Collectively, these data indicate that MCAM identifies *Lepr*-lineage proliferating CAFs in AOM/DSS tumors.

Increased MCAM Expression Is Associated With CMS4 and Predicts Poor Survival in Patients With CRC

We investigated the clinical significance of MCAM expression in CRC patients. Consistent with the observed up-regulation of MCAM during mouse colorectal tumorigenesis, MCAM expression was increased in the human adenoma-carcinoma sequence (Figure 5*A* and *B*). Analyses of expression microarray data from human colorectal tissues also showed that *MCAM* transcripts were elevated during colorectal carcinogenesis (Supplementary Figure 18*A* and *B*). Furthermore, scRNA-seq data from human colorectal tissues[2] demonstrated that, among fibroblast subpopulations, *MCAM* expression was increased in pericytes during carcinogenesis (Supplementary Figure 18*C* and *D*).

Analyses of the TCGA data set showed that the highest expression of *MCAM* was observed in poor-prognosis immunosuppressive CMS4 tumors (Figure 5*C*). Given that TGF-β signaling activation is a defining characteristic of CMS4 CRC,[21] we reasoned that TGF-β might up-regulate *MCAM* expression. In keeping with our hypothesis, stimulation of a mouse colonic fibroblast cell line, YH2 cells, with recombinant TGF-β1 enhanced *Mcam* transcript levels and a TGF-β target gene, *Acta2* (Figure 5*D*). This was rescued by co-treatment with galunisertib, a specific inhibitor for TGF-β receptor 1. Consistent herewith, scRNA-seq analysis of human colorectal CAFs,[2] as well as bulk CRC tissue analysis of TCGA and expression microarray data, showed positive correlations between *MCAM* and *ACTA2* expression (Figure 5*E*; Supplementary Figure 19).

Next, to confirm the clinical association between MCAM expression and survival, we performed MCAM immunohistochemistry with the use of tissue microarrays from our own independent cohort of 101 CRC patients. Consistent with a previous paper,[27] high MCAM expression was an independent prognostic factor for poor overall survival in CRC patients (Figure 5*F* and *G*; Supplementary Tables 2 and 3). Moreover, analyses of 4 independent CRC data sets confirmed that high *MCAM* expression was inversely associated with survival (Supplementary Figure 20). Taken together, these data indicate that high MCAM expression driven, at least in part, by TGF-β predicts poor prognosis in human CRC.

Genetic Deletion of Stromal Mcam Inhibits Colorectal Tumorigenicity and Improves Survival via Decreased NF-κB–IL34/CCL8–Mediated Macrophage Recruitment

Finally, to delineate the mechanism by which MCAM contributes to CRC progression, we generated *Mcam*-knockout mice by means of CRISPR/Cas9-mediated genome engineering (Supplementary Figure 21*A*) and colonoscopically injected luciferase-expressing AKP tumoroids into the colons of *Mcam*-knockout and wild-type mice (Figure 6*A*). In this mouse model, more than half of MCAM$^+$ cells were ACTA2$^+$ CAFs (Supplementary Figure 21*B* and *C*). Consistent with our earlier *MCAM* expression and survival analyses from human CRC, *Mcam*-knockout mice showed prolonged survival after tumoroid injection (Figure 6*B*). *Mcam*-knockout mice also demonstrated reduced tumoroid-derived luciferase signals according to in vivo imaging system, decreased tumor volumes, and colonoscopic tumor scores (Figure 6*C*–*F*; Supplementary Figure 22*A* and *B*). In keeping with this, tumors from *Mcam*-knockout mice showed reduced histologic tumor area and Ki67 labeling (Supplementary Figure 22*C*–*F*).

Immunohistochemistry for various immune cell markers revealed that infiltration of CD68$^+$ macrophages and CD11b$^+$ myeloid-derived cells was decreased in tumors from *Mcam*-knockout mice (Figure 6*G* and *H*). This was accompanied by decreased FOXP3$^+$ regulatory T cells and increased CD8$^+$

Figure 5. High stromal MCAM expression driven, in part, by transforming growth factor (TGF) β is associated with poor survival in patients with CRC. (*A, B*) Immunohistochemistry (IHC) for MCAM in human colorectal samples. (*A*) Representative pictures. (*B*) MCAM positivity in total stromal cells (visualized by hematoxylin counterstaining). 3 HPFs (×400)/patient, 4–5 patients each. (*C*) Violin plots showing *MCAM* expression levels in 4 CMSs. n = 76, 220, 72, and 143 patients (CMS1–4). TCGA, The Cancer Genome Atlas. (*D*) A mouse colonic fibroblast cell line, YH2, was incubated with vehicle, recombinant TGF-β1, or recombinant TGF-β1 + TGF-β1 receptor inhibitor (galunisertib) for 24 hours, followed by quantitative reverse-transcription polymerase chain reaction. Mean ± SEM. n = 3. DMSO, dimethylsulfoxide. (*E*) Single-cell RNA sequencing data show that *MCAM* transcript levels are positively correlated with *ACTA2* expression in colorectal CAFs. n = 1854 CAFs. Solid line, linear regression. (*F, G*) MCAM IHC in a CRC tissue microarray (*F*) Representative images and scoring system. (*G*) Kaplan-Meier survival curves. Scale bars, 50 μm. Kruskal-Wallis test followed by Dunn's multiple comparisons test (*B* and *C*), 1-way analysis of variance followed by Tukey's post hoc multiple comparison test (*D*), Spearman correlation (*E*), and log-rank test (*G*): ****$P < 0.0001$; *$P = 0.0124$. Abbreviations as in Figures 1 and 4.

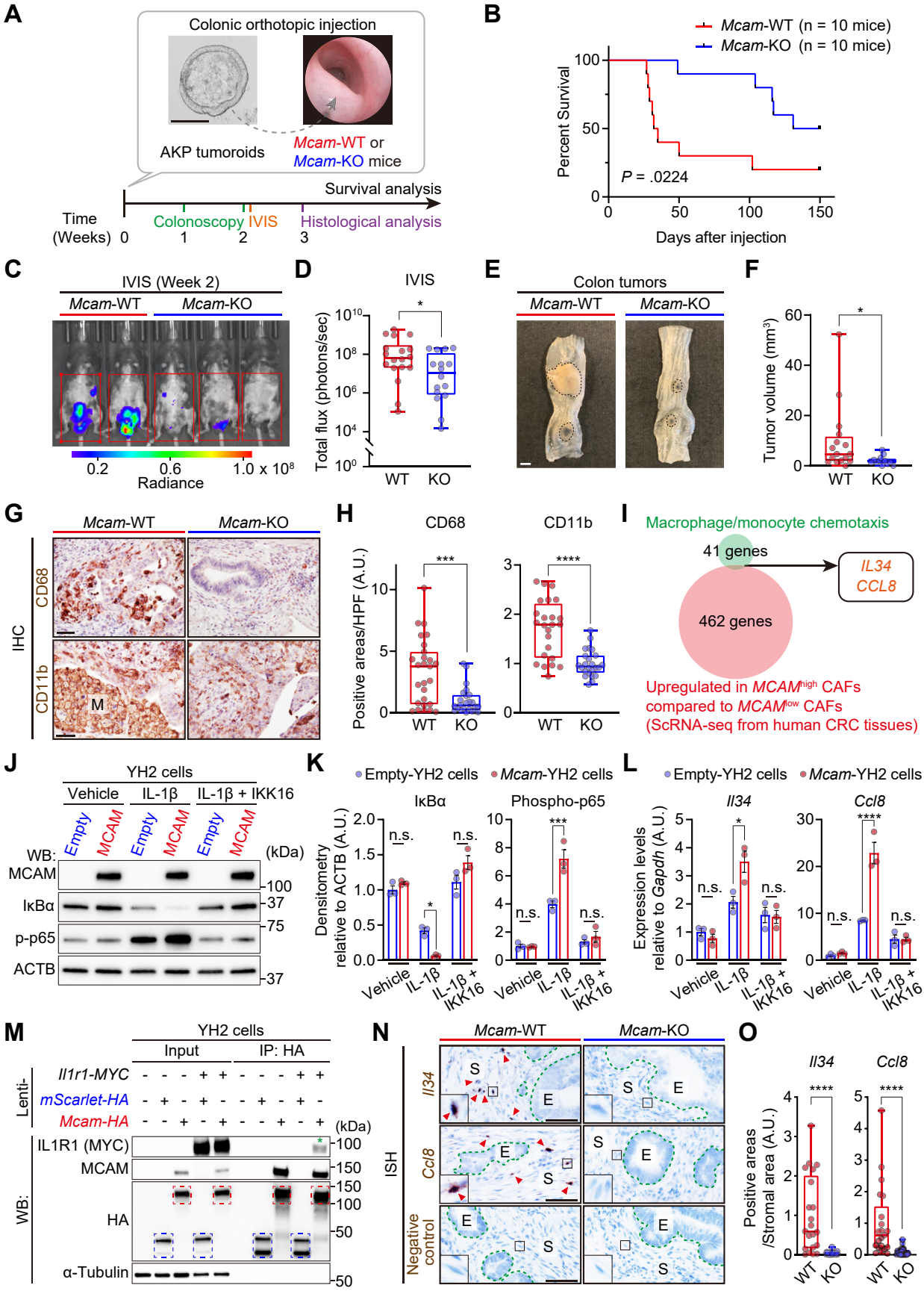
A
Colonic orthotopic injection
AKP tumoroids
Mcam-WT or
Mcam-KO mice
Survival analysis
Time
(Weeks) 0
Colonoscopy IVIS
1
2
Histological analysis
3
B
Mcam-WT (n = 10 mice)
Mcam-KO (n = 10 mice)
Percent Survival
P = .0224
Days after injection
C
IVIS (Week 2)
Mcam-WT
Mcam-KO
Radiance
D
IVIS
Total flux (photons/sec)
WT
KO
E
Colon tumors
Mcam-WT
Mcam-KO
F
Tumor volume (mm3)
WT
KO
G
Mcam-WT
Mcam-KO
IHC
CD68
CD11b
M
H
CD68
CD11b
Positive areas/HPF (A.U.)
WT
KO
I
Macrophage/monocyte chemotaxis
41 genes
IL34
CCL8
462 genes
Upregulated in MCAMhigh CAFs
compared to MCAMlow CAFs
(ScRNA-seq from human CRC tissues)
J
YH2 cells
Vehicle
IL-1β
IL-1β + IKK16
Empty
MCAM
WB:
MCAM
IκBα
p-p65
ACTB
(kDa)
K
Empty-YH2 cells
Mcam-YH2 cells
IκBα
Phospho-p65
Densitometry relative to ACTB (A.U.)
n.s.
Vehicle
IL-1β
IL-1β + IKK16
L
Il34
Ccl8
Expression levels relative to Gapdh (A.U.)
M
YH2 cells
Input
IP: HA
Lenti-
Il1r1-MYC
mScarlet-HA
Mcam-HA
IL1R1 (MYC)
MCAM
HA
α-Tubulin
N
Mcam-WT
Mcam-KO
ISH
Il34
Ccl8
Negative control
S
E
O
Il34
Ccl8
Positive areas /Stromal area (A.U.)

cytotoxic T cells in *Mcam*-knockout mice (Supplementary Figure 23*A* and *B*). In our mouse model, we did not observe alterations in $CD31^+$ vasculature density or $ACTA2^+$ CAF area by *Mcam* knockout (Supplementary Figure 23*C*–*F*). Normal adult colons from *Mcam*-knockout mice did not show altered Ki67 labeling or crypt density or length (Supplementary Figure 24). This suggests that, in *Mcam*-knockout mice, there are no pre-existing changes in normal colon morphogenesis that lead to the altered tumor size.

Consistent with our mouse immunophenotyping data, gene set enrichment analysis with the use of TCGA data revealed positive enrichment of macrophage/monocyte chemotaxis genes in $MCAM^{high}$ cancers compared with $MCAM^{low}$ tumors (Supplementary Figure 25). We hypothesized that $MCAM^+$ CAFs might promote tumor-associated macrophage (TAM) recruitment, contributing to the immunosuppressive tumor microenvironment. To identify macrophage/monocyte chemoattractants secreted by $MCAM^+$ CAFs, we first performed differential gene expression analysis with the use of scRNA-seq data from human CRC[2] and found that 462 genes were up-regulated in $MCAM^{high}$ CAFs compared with $MCAM^{low}$ CAFs (Figure 6*I*). Next, using gene ontologies, we examined transcripts encoding cytokines and chemokines involved in macrophage/monocyte chemotaxis. This analysis identified *IL34* and *CCL8* as genes with roles in TAM recruitment that are up-regulated in $MCAM^{high}$ CAFs.

Next, to assess whether MCAM could promote IL34 and CCL8 expression, we overexpressed MCAM in YH2 cells by means of lentiviral transduction and stimulated MCAM-YH2 cells with recombinant interleukin (IL) 1β, which is known to induce IL34 and CCL8 expression in fibroblasts.[28,29] As expected, IL1β–treated MCAM-YH2 cells showed decreased IκBα expression, increased phosphorylation of NF-κB (p65), and enhanced luciferase signals from NF-κB–responsive elements, leading to up-regulation of *Il34* and *Ccl8* (Figure 6*J*-*L*; Supplementary Figure 26). These alterations were rescued by co-treatment with IKK16, a selective inhibitor for IκB kinase. We reasoned that MCAM might act as a co-receptor for IL1β receptor, IL1R1, to potentiate IL1β–NF-κB–IL34/CCL8 signaling. To this end, we lentivirally transduced YH2 cells with MCAM-hemagglutinin (HA) epitope tag or, as a control, mScarlet-HA, and performed immunoprecipitation with an anti-HA antibody. The co-immunoprecipitation revealed that MCAM interacted with IL1R1 (Figure 6*M*). Reciprocal co-immunoprecipitation of MYC-tagged IL1R1 with the use of an anti-MYC antibody verified the interaction of IL1R1 with MCAM (Supplementary Figure 27). In line with our in vitro data, tumors from *Mcam*-knockout mice showed lower stromal expression of *Il34* and *Ccl8* (Figure 6*N* and *O*), accompanied by decreased NF-κB phosphorylation (Supplementary Figure 28). In human CRC, TCGA and expression microarray data confirmed that *MCAM* expression was positively correlated with *IL34* and *CCL8*, as well as *CD68* and *ITGAM* (CD11b) expression (Supplementary Figure 29). Collectively, our data indicate that MCAM alters the immune microenvironment and accelerates CRC progression, in part, through increased TAM recruitment mediated by IL1R1–NF-κB–IL34/CCL8 signaling.

Discussion

In this study, we have shown that about 75% of $ACTA2^+$ CAFs in CRC were generated through proliferation, with the remaining 25% acquired through new or preserved ACTA2 expression in existing fibroblasts (ie, activation). Most proliferating $ACTA2^+$ CAFs were derived from intestinal *Lepr*-lineage stromal cells. These $Lepr^+$ pericryptal fibroblasts are also the chief origin of proliferating $MCAM^+$ CAFs. High stromal MCAM expression is associated with poor clinical outcomes in patients with CRC. Furthermore, transgenic knockout of *Mcam* in the colorectal tumor microenvironment limits tumor growth and improves

Figure 6. Stromal MCAM promotes CRC progression via IL1R1-p65-IL34/CCL8 signaling–mediated macrophage recruitment. (*A*) Experimental scheme showing orthotopic injection of $Apc^{\Delta/\Delta}$, $Kras^{G12D/\Delta}$, $Trp53^{\Delta/\Delta}$ CRC organoids (AKP tumoroids) into the colon. (*B*) Kaplan-Meier survival curves. (*C, D*) Luciferase signals from AKP tumoroids were assessed with the use of IVIS. 18 *Mcam*-WT and 16 *Mcam*-KO mice. (*E, F*) Macroscopic evaluation of colon tumors, harvested 3 weeks after tumoroid injection. (*E*) Representative pictures. *Dotted lines* indicate tumors. (*F*) Quantification of tumor volumes. 2 injections/mouse, 8 *Mcam*-WT and 6 *Mcam*-KO mice. (*G, H*) Immunohistochemistry (IHC) for CD68 and CD11b. (**G**) Representative pictures. M, macrophages as assessed by morphology. (*H*) DAB-positive areas. A.U., arbitrary units. (*I*) Venn diagram showing the overlap of 41 macrophage/monocyte chemoattractant genes identified by means of Gene Ontologies and 462 genes up-regulated in $MCAM^{high}$ CAFs compared with $MCAM^{low}$ CAFs (scRNA-seq data from GSE132465). (*J, K, L*) Lentivirus-mediated overexpression of MCAM augments IL1β-p65-*Il34*/*Ccl8* signaling in YH2 cells. MCAM-overexpressing or empty YH2 cells were stimulated with recombinant IL1β, followed by WB (*J*, *K*) and quantitative reverse-transcription polymerase chain reaction. (*L*). Mean ± SEM. n = 3 each. p-p65, phosphorylated p65. (*M*) Immunoprecipitation (IP) for MCAM-hemagglutinin (HA) tag with an anti-HA antibody, followed by WB. A *green asterisk* denotes the interaction of MCAM-HA with IL1R1. An anti-MYC antibody was used to detect IL1R1 protein tagged with MYC. *Blue and red dotted boxes* indicate mScarlet-HA and MCAM-HA proteins, respectively. (*N, O*) In situ hybridization (ISH) for *Il34*, *Ccl8*, and a negative control probe (bacterial *DapB* gene) (*N*) Representative pictures. *Green dotted lines* indicate borders between stromal (S) and epithelial (E) areas (visualized by means of hematoxylin counterstaining). *Red arrowheads* denote $Il34^+$ or $Ccl8^+$ stromal cells. (*O*) DAB^+ areas in the tumor stroma. Scale bars, 200 μm (*A*), 2 mm (*E*), 50 μm (*G* and *N*). All histopathologic analyses were performed with the use of mice killed 3 weeks after tumoroid injection. 3 HPFs (×400)/tumor, 1–2 tumors/mouse, 5 mice each group (*H* and *O*). Log-rank test (*B*), 2-tailed unpaired *t* test with Welch's correction (*D*), Mann-Whitney *U* test (*F*, *H*, and *O*), and 2-way analysis of variance followed by Tukey's post hoc multiple comparison test (*K* and *L*): ****$P \leq 0.0001$; ***$P \leq 0.001$; *$P \leq 0.05$; ns, $P > 0.05$. AU, arbitrary units; DAB, 3,3′-diaminobenzidine; KO, knockout; IVIS, in vivo imaging system; WB, Western blotting; WT, wild type; other abbreviations as in Figures 1 and 4.

survival by modifying TAM recruitment and immune landscapes. These data suggest that MCAM, a prominent cell surface protein, could prove to be a valuable novel stromal target in the prevention and treatment of CRC.

Several studies have indicated that recruitment from the bone marrow could contribute to CAFs in mouse models of cancers such as gastric and breast cancer.[8,30] In contrast, one paper demonstrated that no *Acta2*-RFP$^+$ CAFs were detected in small intestinal tumors developed in a parabiosis study of an *Apc*$^{Min/+}$ with an *Acta2*-RFP mouse.[10] In agreement with this, we found that no ACTA2$^+$ CAFs were derived from the bone marrow in an AOM/DSS model of CRC. To our knowledge, our study is the first to examine bone marrow contribution to CAFs in tumors in the mouse colon. Human studies using secondary tumors (including colorectal neoplasias) developed after sex-mismatched bone marrow transplantation also indicated that bone marrow–derived cells are not a major contributor to ACTA2$^+$ CAFs.[9,31] It is plausible, and indeed likely, that the origins and contributions of CAFs are context dependent, depending on cancer stage, cancer genetics, and organ-specific microenvironment.

Intestinal normal and neoplastic epithelium develop from stem-progenitor cell hierarchies.[32] Analogously to this, we have previously shown that *Grem1*$^+$ intestinal reticular stromal cells identify connective tissue stem cells in the normal small intestine.[23] Here, our data indicate that the majority of CRC CAFs, however, arise not from *Grem1*$^+$ cells, but from intestinal *Lepr*-lineage pericryptal cells. Interestingly, a recent paper found that *Gli1*$^+$ pancreatic stellate cells could contribute to approximately half of ACTA2$^+$ CAFs in a mouse model of pancreatic cancer.[33] Further research is required to determine the hierarchic or overlapping relationship between *Lepr*-lineage and *Gli1*-lineage CAFs in different tissues in health and neoplasia.

One limitation of the present study is that we were not able to ascertain whether *Lepr*-lineage CAFs display cellular plasticity during cancer development, as has been shown to occur in cancer stem cells,[32] or whether they undergo an irreversible "lineage-restricted" differentiation. Given that CAFs are considered to exhibit tumor stage–dependent phenotypes,[1,34] it is conceivable that *Lepr*-lineage CAFs could adapt to dynamic phenotypic shifts during colorectal carcinogenesis and co-evolve with epithelial genetic events.

Another limitation of this study is that we have not determined whether MCAM expression is induced by TGF-β in *Lepr*-lineage fibroblasts during colorectal tumorigenesis, despite showing that TGF-β up-regulates *Mcam* expression in colonic fibroblasts in vitro. TGF-β signaling plays a key role in differentiation of *Tcf21*$^+$ hepatic stellate cells to ACTA2$^+$ CAFs, thereby promoting liver tumor progression.[35] Further research is warranted to investigate whether conditional knockout of a TGF-β receptor in *Lepr*-lineage cells could suppress MCAM expression and thus attenuate cancer progression in a mouse model of CRC.

This work also demonstrated that MCAM is an attractive therapeutic target that modifies the immunosuppressive milieu through augmenting NF-κB signaling, key signaling that defines inflammatory phenotypes in CAFs.[6,36,37] Excitingly, MCAM-neutralizing antibodies show promising results in restraining cancer progression in preclinical models, including an AOM/DSS model.[17,18] Future research should focus on investigating whether co-treatment of the MCAM-neutralizing antibody and an immune checkpoint inhibitor could unleash a cytotoxic immune response against immunologically "cold" cancers that are resistant to immunotherapies.

In conclusion, our data show that *Lepr*-lineage intestinal stromal cells, resident at the pericryptal base in the normal colon, proliferate in colorectal carcinogenesis to generate MCAM$^+$ CAFs. We also show that MCAM is an important factor in sculpting the detrimental immune microenvironment responsible for driving colorectal carcinogenesis and the associated poor patient outcome. In the future, approaches to reduce the expansion of *Lepr*$^+$ pericryptal cells, prevent their differentiation into MCAM$^+$ CAFs, and inhibit the activity of MCAM-mediated NF-κB signaling axis in mature CAFs may all have considerable clinical value in the treatment of colorectal cancer.

Supplementary Material

Note: To access the supplementary material accompanying this article, visit the online version of Gastroenterology at www.gastrojournal.org, and at https://doi.org/10.1053/j.gastro.2021.11.037.

References

1. Kobayashi H, Enomoto A, Woods SL, et al. Cancer-associated fibroblasts in gastrointestinal cancer. Nat Rev Gastroenterol Hepatol 2019;16:282–295.
2. **Lee HO, Hong Y, Etlioglu HE**, et al. Lineage-dependent gene expression programs influence the immune landscape of colorectal cancer. Nat Genet 2020;52:594–603.
3. Kobayashi H, Gieniec KA, Wright JA, et al. The balance of stromal BMP signaling mediated by GREM1 and ISLR drives colorectal carcinogenesis. Gastroenterology 2021;160:1224–1239.e30.
4. Ozdemir BC, Pentcheva-Hoang T, Carstens JL, et al. Depletion of carcinoma-associated fibroblasts and fibrosis induces immunosuppression and accelerates pancreas cancer with reduced survival. Cancer Cell 2014;25:719–734.
5. Bartoschek M, Oskolkov N, Bocci M, et al. Spatially and functionally distinct subclasses of breast cancer-associated fibroblasts revealed by single cell RNA sequencing. Nat Commun 2018;9:5150.
6. Biffi G, Oni TE, Spielman B, et al. IL1-induced JAK/STAT signaling is antagonized by TGFβ to shape CAF heterogeneity in pancreatic ductal adenocarcinoma. Cancer Discov 2019;9:282–301.
7. Rhim AD, Mirek ET, Aiello NM, et al. EMT and dissemination precede pancreatic tumor formation. Cell 2012;148:349–361.
8. **Quante M, Tu SP**, Tomita H, et al. Bone marrow–derived myofibroblasts contribute to the mesenchymal stem cell

niche and promote tumor growth. Cancer Cell 2011; 19:257–272.
9. Worthley DL, Ruszkiewicz A, Davies R, et al. Human gastrointestinal neoplasia-associated myofibroblasts can develop from bone marrow–derived cells following allogeneic stem cell transplantation. Stem Cells 2009; 27:1463–1468.
10. Arina A, Idel C, Hyjek EM, et al. Tumor-associated fibroblasts predominantly come from local and not circulating precursors. Proc Natl Acad Sci U S A 2016; 113:7551–7556.
11. El Agha E, Kramann R, Schneider RK, et al. Mesenchymal stem cells in fibrotic disease. Cell Stem Cell 2017;21:166–177.
12. Ding L, Morrison SJ. Haematopoietic stem cells and early lymphoid progenitors occupy distinct bone marrow niches. Nature 2013;495:231–235.
13. Zhou BO, Yue R, Murphy MM, et al. Leptin-receptor–expressing mesenchymal stromal cells represent the main source of bone formed by adult bone marrow. Cell Stem Cell 2014;15:154–168.
14. Decker M, Martinez-Morentin L, Wang G, et al. Leptin-receptor–expressing bone marrow stromal cells are myofibroblasts in primary myelofibrosis. Nat Cell Biol 2017;19:677–688.
15. Corselli M, Chin CJ, Parekh C, et al. Perivascular support of human hematopoietic stem/progenitor cells. Blood 2013;121:2891–2901.
16. Brechbuhl HM, Finlay-Schultz J, Yamamoto TM, et al. Fibroblast subtypes regulate responsiveness of luminal breast cancer to estrogen. Clin Cancer Res 2017; 23:1710–1721.
17. **Wang Z, Xu Q**, Zhang N, et al. CD146, from a melanoma cell adhesion molecule to a signaling receptor. Signal Transduct Target Ther 2020;5:148.
18. **Xing S, Luo Y**, Liu Z, et al. Targeting endothelial CD146 attenuates colitis and prevents colitis-associated carcinogenesis. Am J Pathol 2014;184:1604–1616.
19. **Zhang M, Yang H, Wan L**, et al. Single-cell transcriptomic architecture and intercellular crosstalk of human intrahepatic cholangiocarcinoma. J Hepatol 2020; 73:1118–1130.
20. Wu SZ, Roden DL, Wang C, et al. Stromal cell diversity associated with immune evasion in human triple-negative breast cancer. EMBO J 2020;39:e104063.
21. **Guinney J, Dienstmann R, Wang X**, et al. The consensus molecular subtypes of colorectal cancer. Nat Med 2015;21:1350–1356.
22. Torres S, Bartolome RA, Mendes M, et al. Proteome profiling of cancer-associated fibroblasts identifies novel proinflammatory signatures and prognostic markers for colorectal cancer. Clin Cancer Res 2013; 19:6006–6019.
23. Worthley DL, Churchill M, Compton JT, et al. Gremlin 1 identifies a skeletal stem cell with bone, cartilage, and reticular stromal potential. Cell 2015;160:269–284.
24. Reichert M, Takano S, von Burstin J, et al. The Prrx1 homeodomain transcription factor plays a central role in pancreatic regeneration and carcinogenesis. Genes Dev 2013;27:288–300.
25. Sancho E, Batlle E, Clevers H. Signaling pathways in intestinal development and cancer. Annu Rev Cell Dev Biol 2004;20:695–723.
26. Espin-Palazon R, Traver D. The NF-κB family: key players during embryonic development and HSC emergence. Exp Hematol 2016;44:519–527.
27. Tian B, Zhang Y, Li N. CD146 protein as a marker to predict postoperative liver metastasis in colorectal cancer. Cancer Biother Radiopharm 2013;28:466–470.
28. Struyf S, van Collie E, Paemen L, et al. Synergistic induction of MCP-1 and -2 by IL-1β and interferons in fibroblasts and epithelial cells. J Leukoc Biol 1998; 63:364–372.
29. Baghdadi M, Umeyama Y, Hama N, et al. Interleukin-34, a comprehensive review. J Leukoc Biol 2018; 104:931–951.
30. **Raz Y, Cohen N**, Shani O, et al. Bone marrow–derived fibroblasts are a functionally distinct stromal cell population in breast cancer. J Exp Med 2018;215:3075–3093.
31. Kurashige M, Kohara M, Ohshima K, et al. Origin of cancer-associated fibroblasts and tumor-associated macrophages in humans after sex-mismatched bone marrow transplantation. Commun Biol 2018;1:131.
32. Batlle E, Clevers H. Cancer stem cells revisited. Nat Med 2017;23:1124–1134.
33. Garcia PE, Adoumie M, Kim EC, et al. Differential contribution of pancreatic fibroblast subsets to the pancreatic cancer stroma. Cell Mol Gastroenterol Hepatol 2020;10:581–599.
34. Friedman G, Levi-Galibov O, David E, et al. Cancer-associated fibroblast compositions change with breast cancer progression linking the ratio of S100A4$^+$ and PDPN$^+$ CAFs to clinical outcome. Nat Cancer 2020; 1:692–708.
35. **Wang SS, Tang XT, Lin M**, et al. Perivenous stellate cells are the main source of myofibroblasts and cancer-associated fibroblasts formed after chronic liver injuries. Hepatology 2021;74:1578–1594.
36. Erez N, Truitt M, Olson P, et al. Cancer-associated fibroblasts are activated in incipient neoplasia to orchestrate tumor-promoting inflammation in an NF-κB–dependent manner. Cancer Cell 2010;17:135–147.
37. Koliaraki V, Pasparakis M, Kollias G. IKKβ in intestinal mesenchymal cells promotes initiation of colitis-associated cancer. J Exp Med 2015;212:2235–2251.

Author names in bold designate shared co-first authorship.

Received March 9, 2021. Accepted November 21, 2021.

Correspondence
Address correspondence to: Daniel L. Worthley, MBBS(Hons), PhD, MPH, FRACP, Group Leader, Gut Health, SAHMRI (5 South), North Terrace, Adelaide, South Australia 5000, Australia. e-mail: dan@colonoscopyclinic.com.au, or Susan L. Woods, PhD, Group Leader, Gut Cancer, University of Adelaide, SAHMRI (5 South), North Terrace, Adelaide, South Australia 5000, Australia. e-mail: susan.woods@adelaide.edu.au, or Atsushi Enomoto, MD, PhD, Professor, Department of Pathology, Nagoya University School of Medicine, 65 Tsurumai-Cho, Showa-Ku, Nagoya, 466-8550, Japan. e-mail: enomoto@iar.nagoya-u.ac.jp.

Acknowledgments
The authors thank Kaori Ushida and Kozo Uchiyama (Nagoya University, Japan) for their technical assistance. The mouse colonic fibroblast cell line YH2 was a kind gift from Professor Antony Burgess (Walter and Eliza Hall Institute of

Medical Research, Australia). We acknowledge the facilities and the scientific and technical assistance of the South Australian Genome Editing (SAGE) Facility, the University of Adelaide, and the South Australian Health and Medical Research Institute. SAGE is supported by Phenomics Australia. Phenomics Australia is supported by the Australian Government through the National Collaborative Research Infrastructure Strategy program.

CRedit Authorship Contributions

Hiroki Kobayashi, MD, PhD (Conceptualization: Equal; Data curation: Equal; Formal analysis: Equal; Funding acquisition: Supporting; Investigation: Equal; Methodology: Equal; Validation: Equal; Visualization: Lead; Writing—original draft: Equal); Krystyna A. Gieniec, PhD (Conceptualization: Equal; Data curation: Equal; Formal analysis: Equal; Funding acquisition: Supporting; Investigation: Equal; Methodology: Equal; Validation: Equal; Writing—review & editing: Supporting); Tamsin RM. Lannagan, PhD (Conceptualization: Equal; Data curation: Equal; Formal analysis: Equal; Investigation: Equal; Methodology: Equal; Validation: Equal; Writing—review & editing: Supporting); Tongtong Wang, BSc (Hons) (Data curation: Supporting; Formal analysis: Supporting; Investigation: Supporting; Methodology: Supporting; Visualization: Supporting; Writing—review & editing: Supporting); Naoya Asai, MD, PhD (Formal analysis: Supporting; Investigation: Supporting; Methodology: Supporting; Supervision: Supporting; Writing—review & editing: Supporting); Yasuyuki Mizutani, MD, PhD (Investigation: Supporting; Methodology: Supporting; Writing—review & editing: Supporting); Tadashi Iida, MD (Investigation: Supporting; Methodology: Supporting; Writing—review & editing: Supporting); Ryota Ando, MD (Investigation: Supporting; Methodology: Supporting; Writing—review & editing: Supporting); Elaine M. Thomas, BSc (Investigation: Supporting; Methodology: Supporting; Writing—review & editing: Supporting); Akihiro Sakai, MD (Investigation: Supporting; Methodology: Supporting; Writing—review & editing: Supporting); Nobumi Suzuki, MD, PhD (Writing—review & editing: Supporting); Mari Ichinose, MD, PhD (Writing—review & editing: Supporting); Josephine A. Wright, PhD (Writing—review & editing: Supporting); Laura Vrbanac, PhD (Methodology: Supporting; Writing—review & editing: Supporting); Jia Q. Ng, PhD (Writing—review & editing: Supporting); Jarrad Goyne, BSc (Hons) (Writing—review & editing: Supporting); Georgette Radford, BSc (Hons) (Investigation: Supporting; Methodology: Supporting; Writing—review & editing: Supporting); Matthew J. Lawrence, MBBS (Writing—review & editing: Supporting); Tarik Sammour, MBChB, PhD (Writing—review & editing: Supporting); Yoku Hayakawa, MD, PhD (Writing—review & editing: Supporting); Sonja Klebe, MD, PhD (Resources: Supporting; Writing—review & editing: Supporting); Alice E. Shin, BMSc (Investigation: Supporting; Writing—review & editing: Supporting); Samuel Asfaha, MD, PhD (Conceptualization: Supporting; Supervision: Supporting; Writing—review & editing: Supporting); Mark L. Bettington, MBBS, PhD, FRCPA (Resources: Supporting; Writing—review & editing: Supporting); Florian Rieder, MD (Writing—review & editing: Supporting); Nicholas Arpaia, PhD (Writing—review & editing: Supporting); Tal Danino, PhD (Writing—review & editing: Supporting); Lisa M. Butler, PhD (Funding acquisition: Supporting; Writing—review & editing: Supporting); Alastair D. Burt, MD, PhD (Supervision: Supporting; Writing—review & editing: Supporting); Simon J. Leedham, MD, PhD (Writing—review & editing: Supporting); Anil K. Rustgi, MD (Writing—review & editing: Supporting); Siddhartha Mukherjee, MD, PhD (Writing—review & editing: Supporting); Masahide Takahashi, MD, PhD (Conceptualization: Supporting; Funding acquisition: Supporting; Supervision: Supporting; Writing—review & editing: Supporting); Timothy C. Wang, MD (Conceptualization: Supporting; Writing—review & editing: Supporting); Atsushi Enomoto, MD, PhD (Conceptualization: Equal; Funding acquisition: Equal; Project administration: Equal; Supervision: Equal; Writing—original draft: Equal); Susan L. Woods, PhD (Conceptualization: Equal; Funding acquisition: Equal; Project administration: Equal; Supervision: Equal; Writing—original draft: Equal); Daniel L. Worthley, MBBS(Hons), PhD, MPH, FRACP (Conceptualization: Equal; Funding acquisition: Equal; Project administration: Equal; Supervision: Equal; Writing—original draft: Equal)

Conflicts of interest

Florian Rieder is a consultant to or on the advisory board of Agomab, Allergan, AbbVie, Boehringer-Ingelheim, Celgene/BMS, CDISC, Cowen, Genentech, Gilead, Gossamer, Guidepoint, Helmsley, Index Pharma, Jannsen, Koutif, Mestag, Metacrine, Morphic, Origo, Pfizer, Pliant, Prometheus Biosciences, Receptos, RedX, Roche, Samsung, Surrozen, Takeda, Techlab, Theravance, Thetis, and UCB. The other authors declare no conflicts.

Funding

This study was supported by grants from the National Health and Medical Research Council (APP1156391 to Daniel L. Worthley and Susan L. Woods; APP1081852 to Daniel L. Worthley, APP1140236 to Susan L. Woods, and APP1099283 to Daniel L. Worthley); Cancer Council SA Beat Cancer Project on behalf of its donors and the State Government of South Australia through the Department of Health (MCF0418 to Susan L. Woods and Daniel L. Worthley and PRF1117 to Lisa M. Butler); a Grant-in-Aid for Scientific Research 26221304 to Masahide Takahashi) commissioned by the Ministry of Education, Culture, Sports, Science and Technology of Japan; AMED-CREST (Japan Agency for Medical Research and Development, Core Research for Evolutional Science and Technology; 20gm0810007h0105 and 20gm1210009s0102 to Atsushi Enomoto); the Project for Cancer Research and Therapeutic Evolution (P-CREATE) from AMED (20cm0106377h0001 to Atsushi Enomoto and 21cm0106704h0002 to Yasuyuki Mizutani); Japan Society for the Promotion of Science Overseas Challenge Program for Young Researchers (to Hiroki Kobayashi), Takeda Science Foundation Fellowship (to Hiroki Kobayashi), Greaton International PhD Scholarship (to Hiroki Kobayashi), and Lions Medical Research Foundation Scholarship (to Krystyna A. Gieniec).

Transcript Profiling

GSE162508.